BBA - Biomembranes 1863 (2021) 183622

Contents lists available at ScienceDirect

BBA - Biomembranes

journal homepage: www.elsevier.com/locate/bbamem

Comparing the interaction of the antibiotic levofloxacin with zwitterionic and anionic membranes: Calorimetry, fluorescence, and spin label studies

Gabriel S. Vignoli Muniz *, Mariana C. Souza, Evandro L. Duarte, M. Teresa Lamy *

Instituto de Física, Universidade de São Paulo, São Paulo, SP CEP 05508-090, Brazil

ARTICLE INFO

Keywords:
Fluoroquinolone
Levofloxacin
DSC
Spin label ESR
Fluorescence spectroscopy
Time-resolved spectroscopy
Membrane binding
DPPC
DPPG

ABSTRACT

The present work compares the interaction of the antibiotic levofloxacin (LVX) with zwitterionic and anionic liposomes composed of 1,2-dipalmitoyl-sn-glycero-3-phosphocholine (DPPC) and 1,2-dipalmitoyl-sn-glycero-3-phospho-(1′-rac-glycerol) (DPPG), respectively. By using differential scanning calorimetry (DSC), and with spin labels incorporated into liposomes at two different depths of the bilayers, we investigated the changes induced on the membrane by increasing concentrations of LVX. Further information was obtained using intrinsic LVX fluorescence. Under the conditions used here, all techniques evinced that LVX has little affinity for DPPC zwitterionic membrane. Opposite to that, LVX exhibits a considerable affinity for anionic bilayers, with membrane partition constants $K_p = (3.3 \pm 0.5) \times 10^2$ and $(4.5 \pm 0.3) \times 10^2$, for gel and fluid DPPG membranes, respectively. On binding to DPPG, LVX seems to give rise to the coexistence of LVX -rich and -poor domains on DPPG membranes, as detected by DSC. At the highest LVX concentration used (20 mol%), DSC trace shows an increase in the cooperativity of DPPG gel-fluid transition, also detected by spin labels as an increase in the bilayer packing. Moreover, LVX does not induce pore formation in either DPPG or POPG vesicles. Considering the possible relevance of LVX-membrane interaction for the biological and toxicological action of the antibiotic, the findings discussed here certainly contribute to a better understanding of its action, and the planning of new drugs.

1. Introduction

Levofloxacin ((*S*)-9-fluoro-2,3-dihydro-3-methyl-l0-(4-methyl-l-piperazinyl)-7-oxo-7H-pyrido [1,2,3-de]-1,4- benzoxazine-6-carboxylic acid hemihydrate) is a synthetic antibiotic belonging to the fluoroquinolone (FQ) family. FQs are based on the chemical structure of nalidixic acid, which shows a moderate antibiotic activity against Gram-negative bacteria [1].

Levofloxacin (LVX) is an optical levogyre isomer of ofloxacin, a second generation FQ. LVX displays an antimicrobial activity broader than ofloxacin, affecting Gram-negative and Gram-positive bacteria. LVX is commonly used in the treatment of serious respiratory tract infections, chronical bronchitis, pneumonia, and acute sinusitis. It is also used to treat conditions such as skin infections, urinary tract infections, and even serious cases of sepsis [1,2].

It is well established that FQs target the bacterial enzymes DNA gyrase and topoisomerase IV [2,3]. These two enzymes form a DNA cleavage complex, which is responsible for controlling DNA tension and topology during essential cellular processes, such as DNA replication and transcription. Additionally, FQs were found to intercalate into the DNA's double helix, acting as a possible physical block for the enzymatic cleavage complex, thus interrupting the proper function of the cell's machinery, ultimately leading to the bacteria's death [4,5].

The FQs intracellular targets implies that the drug needs to cross the bacterial envelope. The process of FQs internalization is not completely understood and it is still a matter of debate [6]. However, different modes for FQs to access the cell cytosol have been proposed [6–10]. Among them, two stand out: a passive diffusion through the plasmatic

Abbreviations: LVX, Levofloxacin; DPPC, 1,2-dipalmitoyl-sn-glycero-3-phosphocholine; DPPG, 1,2-dipalmitoyl-sn-glycero-3-phospho-(1′-rac-glycerol); POPC, palmitoyl-2-oleoyl-*sn*-glycero-3-phosphocholine; POPG, 1-palmitoyl-2-oleoyl-sn-glycero-3-phospho-(1′-rac-glycerol); LUVs, large unilamellar vesicles; DSC, differential scanning calorimetry; ESR, electron spin resonance; TCSPC, time-correlated single photon counting technique; TR, Time-resolved; FQ, fluorescence, fluoroquinolone; CPX, ciprofloxacin; NFX, norfloxacin; *n*-PCSL, $n = 5$ or 16, spin labels 1-palmitoyl-2-(*n*-doxylstearoyl)-*sn*-glycero-3-phosphocholine; S_{eff}, effective order parameter; $2A_{max}$, maximum hyperfine splitting; CF, 5(6)-Carboxyfluorescein.

* Corresponding authors.
E-mail addresses: gvignoli@if.usp.br (G.S. Vignoli Muniz), mtlamy@usp.br (M.T. Lamy).

https://doi.org/10.1016/j.bbamem.2021.183622
Received 26 January 2021; Received in revised form 30 March 2021; Accepted 31 March 2021
Available online 15 April 2021
0005-2736/© 2021 Elsevier B.V. All rights reserved.

membrane and an active transport mediated by porin channels. It has been suggested that only uncharged FQ species can easily translocate through the plasmatic membrane, without membrane receptors, based on data with zwitterionic giant unilamellar vesicles (GUVs) and molecular dynamics simulations [9,11]. However, it is well established that porin channels are essential for FQs bacteria uptake, but the exact mechanism is not yet completely understood [6,7]. The interaction of the drug with the lipid/porin interface might be important for the FQ internalization, with both porin and lipid pathways involved in the drug incorporation [6,12,13]. Accordingly, drug-lipid interaction might modulate the antibiotic internalization.

The presence of multiple proton binding sites makes FQs acid-basic equilibrium quite complex [14]. Nonetheless, most of the FQs are zwitterionic at physiological pH. Additionally, FQs display different degrees of lipophilicity, what is crucial for their interaction with amphipathic molecules [15,16].

Accordingly, the interaction between FQs and lipids, or amphiphilic aggregates, has been found to be extremely dependent upon the FQ structures. At physiological pH, FQs seems to display a stronger interaction with anionic than with zwitterionic or non-ionic amphiphilic aggregates [17,18]. For example, ciprofloxacin (CPX), a second generation FQ, was found not to disturb the phase transition of zwitterionic bilayers of 1,2-dipalmitoyl-sn-glycero-3-phosphocholine (DPPC), but to interact and cause a relevant effect on the phase transition of anionic liposomes composed of 1,2-dipalmitoyl-sn-glycero-3-phospho-(1′-rac-glycerol) (DPPG), as indicated by infrared spectroscopy experiments [18].

In the same trend, zwitterionic norfloxacin (NFX), another FQ of the second generation, showed a high affinity for anionic micelles of sodium dodecyl sulfate (SDS), whereas micelles of non-ionic surfactant Tween 20 did not promote any change in NFX optical properties, thus indicating that NFX did not bind Tween 20 [17]. It has been proposed that the interaction of anionic polar head groups of amphipathic molecules with FQs is essential for their binding and stability [17–19]. On the other hand, the FQ ofloxacin, which is also zwitterionic at neutral pH, and protonates at lower pH values, was found to disturb zwitterionic DPPC membranes [20].

Hence, the interaction of different FQs with anionic and zwitterionic lipid membranes is depend on their hydrophobic/hydrophilic characteristic and on their acid/basic equilibrium, for instance see Ref. [9,16] and references therein.

Concerning LVX, Langmuir monolayers composed of DPPC-LVX or DPPC-1-palmitoyl-2-oleoyl-*sn*-glycero-3-phosphocholine (POPC)-LVX presented changes in their compressibility, suggesting that LVX is acting close to the polar headgroups and interacting with zwitterionic lipids [21,22]. The interaction of a set of non-membrane targeting antibiotic, including LVX, with stack anionic lipids was investigated through X-ray diffraction. Regarding LVX, the results suggested that LVX binds anionic

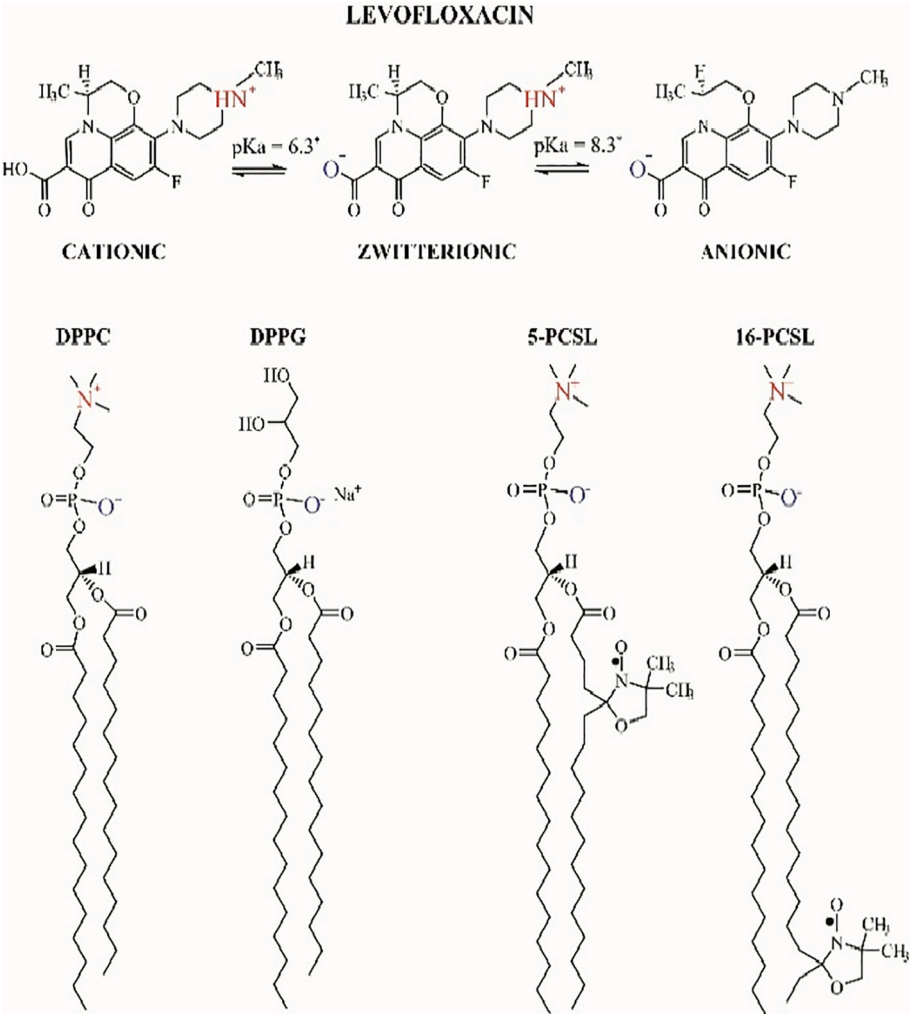

Fig. 1. At the top, schemes of the three different ionic species of levofloxacin, cationic, zwitterionic and anionic. At the bottom, the chemical structures of the zwitterionic lipid DPPC, the anionic lipid DPPG, and the paramagnetic probes 5-PCSL and 16-PCSL. The levofloxacin pK_a values are indicated in the figure. * Ref. [31].

membranes and affects its organization both at the level of the polar headgroups and at the inner core of the bilayer [23].

It is well known that whereas healthy mammalian cells display zwitterionic lipids in their outer leaflet, prokaryotic membranes display anionic polar head groups in its outer membrane [24]. Hence, the study of the interaction of FQs with different lipids may provide information about non-specific drug effects, secondary effects, bioavailability, and FQs accumulation within bacteria cells [21–24]. Additionally, in terms of drug-membrane binding, the interaction between drugs and lipids is essential for the engineering of drug-delivery systems [29,30].

To the best of our knowledge, there is little information in the literature about the interaction of LVX with liposomes, especially in terms of LVX-membrane binding and the LVX effect on the thermotropic and structural properties of lipid bilayers. Therefore, the aim of this work is to perform a comparative investigation on the interaction of LVX at physiological pH (7.4) with liposomes composed of zwitterionic lipids, DPPC, and anionic lipids, DPPG (Fig. 1), as simple mimetic systems of healthy mammalian and bacterial membranes, respectively.

By using differential scanning calorimetry (DSC), and spin labels embedded into the vesicles at different depths of the bilayer, we monitored how increasing concentrations of LVX change the structure and affect the thermotropic behavior of the bilayers. Additionally, we investigated if LVX could induce pore formation in ionic liposomes, through the measurement of the leakage of entrapped carboxyfluorescein (CF), a fluorescent dye.

Complementarily, intrinsic LVX fluorescence gave us the opportunity to monitor possible changes occurring on the antibiotic due to the presence of ionic liposomes, and to determine the affinity of LVX for the different liposomes. Under the conditions used in this work, we do not observe any indication that LVX binds to DPPC zwitterionic liposomes. Opposite to that, LVX binds to anionic DPPG, and the affinity of the antibiotic for DPPG was quantified by the determination of an apparent partition constant. Furthermore, our results indicate that under DPPG-binding the LVX carboxyl ion is mostly neutralized (Fig. 1).

2. Materials & methods

2.1. Chemical and reagents

1,2-dipalmitoyl-sn-glycero-3-phosphocholine (DPPC), sodium salt of 1,2-dipalmitoyl-sn-glycero-3-phospho-(1′-rac-glycerol) (DPPG), 1-palmitoyl-2-oleoyl-glycero-3-phosphocholine (POPC), sodium salt of 1-palmitoyl-2-oleoyl-sn-glycero-3-phospho-(1′-rac-glycerol) (POPG), and spin labels 1-palmitoyl-2-(*n*-doxylstearoyl)-*sn*-glycero-3-phosphocholine (*n*-PCSL, $n = 5$ or 16) were acquired from Avanti Polar Lipids. Levofloxacin (LVX), 4-(2-hydroxyethyl)-1-piperazineethanesulfonic acid (HEPES), Sephadex-G25 columns, 5(6)-Carboxyfluorescein (CF), ethylenediaminetetraacetic acid (EDTA), glucose, ammonium molybdate, citric acid, perchloric acid, sodium phosphate monobasic monohydrate, boric acid, acetic acid sodium salt trihydrate, sodium hydroxide (NaOH), hydrochloric acid (HCL), chloroform, methanol, and sodium chloride (NaCl) were purchased from Merck (St Louis, MO). All water solutions or dispersions were prepared using Milli-Q water.

2.2. Large unilamellar vesicle (LUV) preparations

Lipids were dissolved in a mixture of chloroform and methanol (6:1). When desired, spin labels 5-PCSL (0.8 mol%) or 16-PCSL (0.3 mol%) were added to the lipid solution, this solution was dried under a flux of ultra-pure nitrogen gas till a thin film of lipids was formed at the bottom of the glass tube. The lipid film was kept under low pressure conditions for a minimum of 3 h to eliminate any trace of organic solvent. Lipid dispersions were prepared by the addition of buffer (10 mmol L^{-1} HEPES, 3 mmol L^{-1} NaCl, pH 7.4) to the lipid film, followed by intense vortexing during 2 min at 60 °C, four times. Finally, lipid dispersions were extruded through polycarbonate filters (mini-extruder by Avanti Polar Lipids, 19 mm membranes with 100 nm pores, 31 times) above the lipid gel−fluid transition temperature (≥ 60 °C), for the formation of large unilamellar vesicles (LUVs). After extrusion, the average diameter of the vesicles was checked using dynamic light scattering, and found to be (110 ± 10) nm. Before and after filtering, a few DPPC and DPPG samples were checked for their phospholipid content through inorganic phosphate assay [32], and the error was always found to be less than 1% of the expected value for samples before filtering, and less than 3% after the filtering process. All lipid dispersions used in this work were freshly prepared on the day the experiments were conducted.

2.3. Levofloxacin film and solutions

LVX was dissolved in chloroform (6 mmol L^{-1}). A desired amount of this solution was placed in a glass tube and dried under a flux of ultra-pure nitrogen gas, thus obtaining an antibiotic film at the bottom of the glass tube. The LVX film was submitted to low pressure conditions for at least 3 h. These LVX films were hydrated with buffer or LUV dispersion followed by an intense vortexing for 2 min at 60 °C, four times, to obtain the desired LVX and/or LVX/lipid molar concentration. Finally, the samples were incubated for 30 min at room temperature before the measurements.

2.4. Differential scanning calorimetry (DSC)

DSC thermograms were obtained with a microcalorimeter (Microcal VP-DSC, Northampton, MA). Each sample was scanned five times. The first scan was performed at 90 °C per hour, and not taken into consideration. The next four scans, two endothermic and two exothermic, were runed at the rate of 20 °C per hour, with temperatures ranging from 15 °C to 60 °C. The scans were found to be fairly reproductible. The sample cell (500 μL) was filled with a 3 mmol L^{-1} lipid dispersion with or without the desired concentration of LVX, as described in Section 2.3. In this work, we often refer to the concentration of LVX as the percentage of the antibiotic with respect to the molar concentration of the lipid (mol % [LVX] = 100 [LVX]/[L]), where [LVX] and [L] are LVX and lipid molar concentrations, respectively. By using MicroCal Origin software, with the additional module for DSC data analysis provided by MicroCal, we determined thermodynamic parameters such as the enthalpy variation (ΔH), the position of the maximum of the gel-fluid temperature transition peak, T_m, and the width at half maximum ($\Delta T_{1/2}$).

2.5. Entrapment of carboxyfluorescein (CF) in LUVs and leakage assay

CF solutions were prepared in buffer pH 8.5. After CF solubilization, the sample pH was readjusted to 7.4 with HCl. Lipid films were hydrated with buffer (10 mmol L^{-1} HEPES, 3 mmol L^{-1} NaCl, 1 mmol L^{-1} EDTA, pH 7.4 solution) containing 50 mmol L^{-1} carboxyfluorescein (CF). The lipid dispersion (~6 mmol L^{-1}) was extruded, as previously described. In order to remove non-encapsulated CF, the lipid dispersion was eluted through a Sephadex-G25 medium column with 10 mmol L^{-1} HEPES, pH 7.4 with 1 mmol L^{1} EDTA, 3 mmol L^{-1} NaCl, and 150 mmol L^{-1} glucose, the latter was added to the buffer to adjust the osmolarity inside and outside the liposomes. Vesicles with encapsulated CF were collected in the void volume of the column. Lipid concentration was determined by inorganic phosphate assay [32].

Lipid dispersion (100 μmol L^{-1}) was placed in quartz cuvettes (1.0 × 1.0 cm, 2.0 mL) and the fluorescent emission measured with a Fluorescence Spectrometer (Varian Cary Eclipse, Santa Clara, CA), with temperatures controlled by a Carry Peltier thermostat. The CF leakage measurements were performed under constant stirring. CF encapsulated in LUVs was used to evaluate the ability of LVX to induce pore formation in the ionic bilayers. At 50 mmol L^{-1} the encapsulated CF is self-quenched, hence virtually non-fluorescent. Due to LVX or detergent action, CF might be released into the aqueous bulk, where dilution occurs, thus yielding an increase of CF fluorescence intensity. CF emission

was continuously recorded in time (one measurement per second), at 25 °C, λ_{exc} = 490 nm and λ_{em} = 512 nm. In all experiments, LVX (20 μmol L^{-1}) was added to the lipid dispersion (100 μmol L^{-1}) at the 1.67 min (100th second), and at the end of the experiment, at the 33.33 min (2000th second), Triton X-100 (18 μL of 10% *w/v*) was injected into the sample to promote complete CF leakage.

The percentage of CF leakage, (%) Leakage, was determined according to the following equation:

$$(\%)\ Leakage(t) = 100 \times \frac{(I(t) - I_0)}{(I_{total} - I_0)} \quad (1)$$

where I(t) is the fluorescence intensity at time t, I_0 is the initial fluorescence, before the antibiotic addition, and I_{total} is the maximum fluorescence obtained after the addition of Triton X-100. The kinetics were performed using liposomes of zwitterionic DPPC or anionic DPPG in the gel phase, at 25 °C. As the experimental procedure with fluid dipalmitoyl bilayers (50 °C) was found to be quite unreliable [33,34], to mimic the fluid phase of the dipalmitoyl membranes, similarly prepared vesicles of POPC or POPG were used at 25 °C.

2.6. Electron spin resonance (ESR) spectroscopy

X-band (9.44 GHz) electron paramagnetic resonance spectra were obtained with a Bruker EMX spectrometer. Field-modulation of 1 or 2 G and microwave power of 5 mW were used. The temperature ranged from 10 °C to 60 °C, controlled by a Bruker BVT-2000 variable temperature device. ESR data were analyzed using the software WINEPR.

The maximum ($2A_{max}$), and inner ($2A_{min}$) hyperfine splittings were measured directly on the ESR spectrum, and, for fluid membranes, the effective order parameter (S_{eff}) and the isotropic hyperfine splitting (a_0) were calculated according to the equations:

$$S_{eff} = \frac{A_{\parallel} - A_{\perp}}{A_{zz} - (1/2)(A_{xx} + A_{yy})} \frac{a_o'}{a_o} \quad (2)$$

where $A_{\parallel} \approx A_{max}$

$$A_{\perp} = A_{min} + 1.4 \left[1 - \frac{A_{\parallel} - A_{min}}{A_{zz} - \left(\frac{1}{2}\right)(A_{xx} + A_{yy})} \right]$$

$$a_0' = 1/3\,(A_{zz} + A_{yy} + A_{xx})$$

$$a_0 = 1/3\,(A_{\parallel} + 2A_{\perp})$$

A_{zz}, A_{xx}, and A_{yy} are the principal values of the hyperfine tensor for 2-doxyl propane, 32.9, 5.9, and 5.4 G, respectively [35,36]. With the spin label 16-PCSL, for gel liposomes, the central line width (ΔH_0) was directly measured on the 16-PCSL ESR spectra (see Fig. 6). At the fluid phase, the amplitude of the three hyperfine lines (h_{+1}, h_0, and h_{-1}) were also measured directly on the ESR spectra (see Fig. 6). For more details, see Ref. [37]. The lipid concentration used was 3 mmol L^{-1}, with or without the desired concentration of LVX,

2.7. Ultraviolet-visible (UV–vis) absorption spectroscopy

Optical absorption spectra were obtained with an UV–vis spectrophotometer (Varian Cary 50, Santa Clara, CA). In all optical experiments, samples were placed in a quartz cuvette (0.2 × 1.0 cm, 400 μL), with the absorption optical pathway of 0.2 cm. The temperature was controlled with a Carry Peltier thermostat.

Samples were prepared according to the following protocol. A LVX film, see Section 2.3, was hydrated with a buffer solution (10 mmol L^{-1} HEPES, 3 mmol L^{-1} NaCl, pH 7.4) to prepare a stock LVX solution, 0.5 mmol L^{-1}. Then, LVX was diluted by using the same buffer and/or using a concentrated LUV dispersion (10 mmol L^{-1}), see Section 2.2, to achieve a LVX concentration of 0.01 mmol L^{-1}, with or without the desired lipid concentration. Next, the sample was quickly vortexed and left to equilibrate at room temperature for 30 min. Then, the sample was placed in the spectrometer previously set-up at 25 °C, corresponding to the gel phase of dipalmitoyl bilayers. Then, to assure the thermal equilibrium, the sample was left for 20 min inside the spectrometer. The optical experiments were conducted in sequence, first the absorption spectrum was registered, then the steady-state fluorescence spectrum, and finally the fluorescence decay was measured. All the instruments were set at 25 °C. At the end, the temperature was increased to 50 °C, corresponding to the fluid phase of dipalmitoyl bilayers, and the same protocol was followed.

Absorbance here is A(λ) = log (I_0(λ)/I(λ)), where I_0 (λ) and I (λ) are the intensities of the light beam before and after crossing the sample, respectively, as measured by the spectrophotometer. Hence, it includes light absorbed and scattered by the sample.

2.8. Stead-state fluorescence spectroscopy

Steady-state fluorescence measurements were performed with a fluorimeter (Varian Eclipse, Santa Clara, CA) with temperatures controlled by a Carry Peltier thermostat. Fluorescence experiments were performed using 400 μl solutions of 0.01 mmol L^{-1} LVX in buffer (10 mmol L^{-1} HEPES, 3 mmol L^{-1} NaCl, pH 7.4) without or with LUVs, as described above. The experiments were conducted with an excitation beam light at 345 nm, with an optical pathway of 0.2 cm, with slits for excitation and for emission of 5 nm. The inner filter correction [38] was applied to all the fluorescent emission spectra by using the following equation:

$$F_{corr}(\lambda) = F_{obs}(\lambda) 10^{(A_{exc}\ l + A_{ems} l')} \quad (3)$$

where F_{corr} (λ) and F_{obs} (λ) are the corrected and observed fluorescence intensities, A_{exc} and A_{ems} are the absorbance per unit of pathway at the excitation and emission wavelengths, respectively. l and l′ are the optical pathway in cm for excitation (0.1 cm), and for emission (0.5 cm), respectively, considering the cuvette center.

Eq. (3) does not consider the dimensions of the excited region, as it is assumed that all emitting fluorophores are at the center of the cuvette. It has been shown that this equation is suitable for the absorbance values used here [39].

To investigate changes in LVX emission due to changes in the buffer acidity, a buffer solution was chosen to cover pH values from 4.5 to 7.5. This universal buffer consists of a mixture of 20 mmol L^{-1} boric acid, 20 mmol L^{-1} sodium phosphate monobasic, and 20 mmol L^{-1} acetic acid sodium salt. By using concentrated solutions of (2 mol L^{-1}) HCl or (2 mol L^{-1}) NaOH the universal buffer pH was adjusted and the emission spectrum of LVX at different pH values was measured under constant temperature (50 °C).

2.9. Time resolved fluorescence spectroscopy

Time-resolved (TR) fluorescence measurements were performed using time-correlated single photon counting technique (TCSPC). The excitation light beam comes from a titanium-sapphire Tsunami 3950 laser from Spectra Physics (Newport Corporation, Irvine, CA, USA), pumped by a solid-state laser Millenia Pro model J80 also from Spectra Physics. The frequency of pulse picker (Spectra Physics model 3980-25) was 8 MHz. The Tsunami was set to give an output of 852 nm and a third harmonic generator BBO crystal (GWN-23PL Spectra Physics) was used to generate the excitation light at 284 nm. Although this is different from the excitation wavelength used in the steady state fluorescence, 345 nm, it also corresponds to an absorption band of LVX (see Fig. SM1), and LVX fluorescence relaxation should not depend on the excitation wavelength [38]. At 284 nm the signal-to-noise was much better than at 345 nm. The

emission was detected at 90 degree from the excitation beam and selected by a monochromator.

By using FAST software supplied by Edinburgh Photonics the data were fitted by applying the model of exponential decays [38] using the following equations:

$$F(\lambda,t) = \sum_{i=1}^{N} \alpha_i e^{-t/\tau_i} \quad (4)$$

$$f_i = \frac{\alpha_i \tau_i}{\sum_j \alpha_j \tau_j}$$

where F(λ,t) is the number of photons emitted at a given wavelength (λ) and time (t), α_i is the pre-exponential factor, τ_i is the lifetime of the i^{th} component of the decay, and f_i is the fraction contribution of the lifetime τ_I to the intensity decay.

The fluorescence decay curves were also evaluated by a global analysis [40], where two lifetimes, corresponding to the LVX lifetime in the aqueous phase (τ_1) and LVX lifetime in the lipid phase (τ_2), were constrained to be the same and used to fit all the decay curves, with different fractional contributions: f_1, and f_2 corresponding to the contributions of the lifetimes relative to LVX in the aqueous and lipid phases, respectively. We determined these latter factors from the best fitting processes which results from the statistical parameter reduced chi-square (χ^2), $0.95 \leq \chi^2 \leq 1.35$. An apparent partition constant (K_p) was determined from the best non-linear fitting process using a conventional isotherm:

$$K_p \equiv \frac{n_L/V_L}{n_{aq}/V_{aq}}$$

$$f_2 = \frac{K_P \gamma_L [L]}{1 + K_P \gamma_L [L]} \quad (5)$$

where n_L, and n_{aq} are the number of moles of LVX in the lipid and aqueous phases, respectively. V_{aq} is the volume of the aqueous phase which is in a good approximation equal to the total volume (V_{total}.), taking into consideration both phases, aqueous and lipid. V_L is the volume of the lipid phase, $V_L = \gamma_L$ [L] V_{total}. $f_2 = [LVX]_L/[LVX]_T$ is the relative fraction of LVX in the lipid phase, γ_L is the molar volume of the phospholipid.

2.10. Reproducibility and sample stability

Every experiment was performed at least three times. Error values account for standard deviations and are presented as error bars when larger than the symbols.

No vesicle precipitation was observed during the experiments. The samples were always visually checked before and after the measurements were taken. For optical absorption and fluorescence measurements, LVX spectrum was quite reproducible after a minimum of 3 h in the cuvette.

3. Results

3.1. Membrane modifications induced by levofloxacin

Membranes composed of one lipid species often have two different thermal phases: a gel and a fluid phase. Within the bilayer, lipid molecules are confined into the two-dimensional plane of the membrane, but in the fluid phase lipids are in a more isotropic motion, wobbling along the axis of the acyl chain, whereas in the gel phase the lipids are more packed and organized, with greater mobility restrictions, therefore in a more anisotropic motion. As exogenous molecules may interact more with lipids in a given phase [41], in this work we investigated the interaction of LVX with ionic gel and fluid liposomes. The two lipid phases would somehow mimic different lipid patches, more or less packed in a biological membrane.

3.1.1. Differential Scanning Calorimetry (DSC)

Lipid melting is a collective process which depends on lipid-lipid interaction, and may be profoundly affected by an exogenous molecule if it interacts with the lipid bilayer. Therefore, DSC technique might provide information about structural modifications induced by the presence of LVX on membranes. FQs present melting temperatures higher than 120 °C. For instance, LVX presents a melting temperature above 220 °C [15,42,43]. Hence, DSC from 15 °C to 60 °C is probing the thermal properties of the lipid bilayers only, and the modifications induced on them by the presence of the antibiotic.

Fig. 2 displays the thermotropic behavior of DPPC (left column) and DPPG (right column) in the absence (a,b) and in the presence of 10 (c,d) and 20 (e,f) mol% of LVX, relative to the lipid concentration, under endothermic (red lines) and exothermic (blue lines) processes. Pure dipalmitoyl lipids display a quite reversible thermal behavior (Fig. 2a, b), as it has been observed before [33,34].

Different from multilamellar dispersions, extruded dispersions of DPPC and DPPG present a very subtle and smooth pre-transition temperature peak around 34 °C, Fig. 2(a,b). Besides, multilamellar dipalmitoyl dispersions present a much more cooperative phase transition, *i.e.*, a width at half maximum ($\Delta T_{1/2}$) much smaller than that found for extruded vesicles here [41].

Table 1 summarizes the thermodynamic parameters determined from the DSC thermograms for both processes, endothermic and exothermic.

Note that T_m and ΔH for pure lipid dispersions are in good accordance with the values previously reported [33,34,44]. The presence of LVX did not cause any significant change on the thermotropic behavior of DPPC dispersions, even in the presence of 20 mol% LVX (Fig. 2, left column, and Table 1). In contrast, the presence of LVX profoundly changes DPPG thermotropic behavior. The presence of 10 mol% of LVX lead to the presence of two thermal peaks (Fig. 2d). It is worthy to note that at this concentration one of the thermal peaks is centered at the same temperature (T_m) as that observed for pure DPPG dispersion (Fig. 2, right column, dotted line), and, like that, is quite reversible, whereas the other thermal peak, at a lower temperature, presents a significative hysteresis under endothermic and exothermic processes, of around 0.5 °C. With the presence of 20 mol% LVX, the peak similar to that observed with pure DPPG disappears, being replaced by just one peak at a somewhat lower temperature, indicating a relatively more cooperative transition (smaller value of $\Delta T_{1/2}$), and displaying endothermic/exothermic processes hysteresis (Table 1).

3.1.2. Carboxyfluorescein (CF) leakage assay

Since DSC thermograms (Fig. 2) showed that LVX induces changes on the thermotropic behavior of anionic DPPG, it was important to inquire if the antibiotic could induce pore formation on the ionic liposomes. CF leakage assay is an efficient methodology to check if an exogenous molecule can disturb liposomes, forming pores. As previously stated, CF is a dye that when entrapped within liposomes at 50 mmol L^{-1} is almost non-fluorescent due to self-quench. If a molecule disturbs the bilayer, causing permanent or temporary pores, allowing the dye to leak into the bulk, its dilution results in an increasing of CF intensity emission. By using this methodology, we investigated if 20 mol% LVX could induce pore formation in gel (25 °C) vesicles composed of DPPC (Fig. 3a) or DPPG (Fig. 3b). Given the spontaneous CF leakage from dipalmitoyl fluid bilayers (see Section 2.5), we used POPC (Fig. 3c) and POPG (Fig. 3d) at 25 °C to mimic the fluid phase of dipalmitoyl bilayers.

The spontaneous CF leakage through gel vesicles of DPPC or DPPG is negligible, it is inferior to 1% after 30 min. Interestingly, the presence of 20 mol% LVX did not have any significant impact on the CF leakage through gel membranes, as can be seen in Fig. 3(a,b).

In the fluid phase, POPC liposomes (Fig. 3c) in the absence of LVX

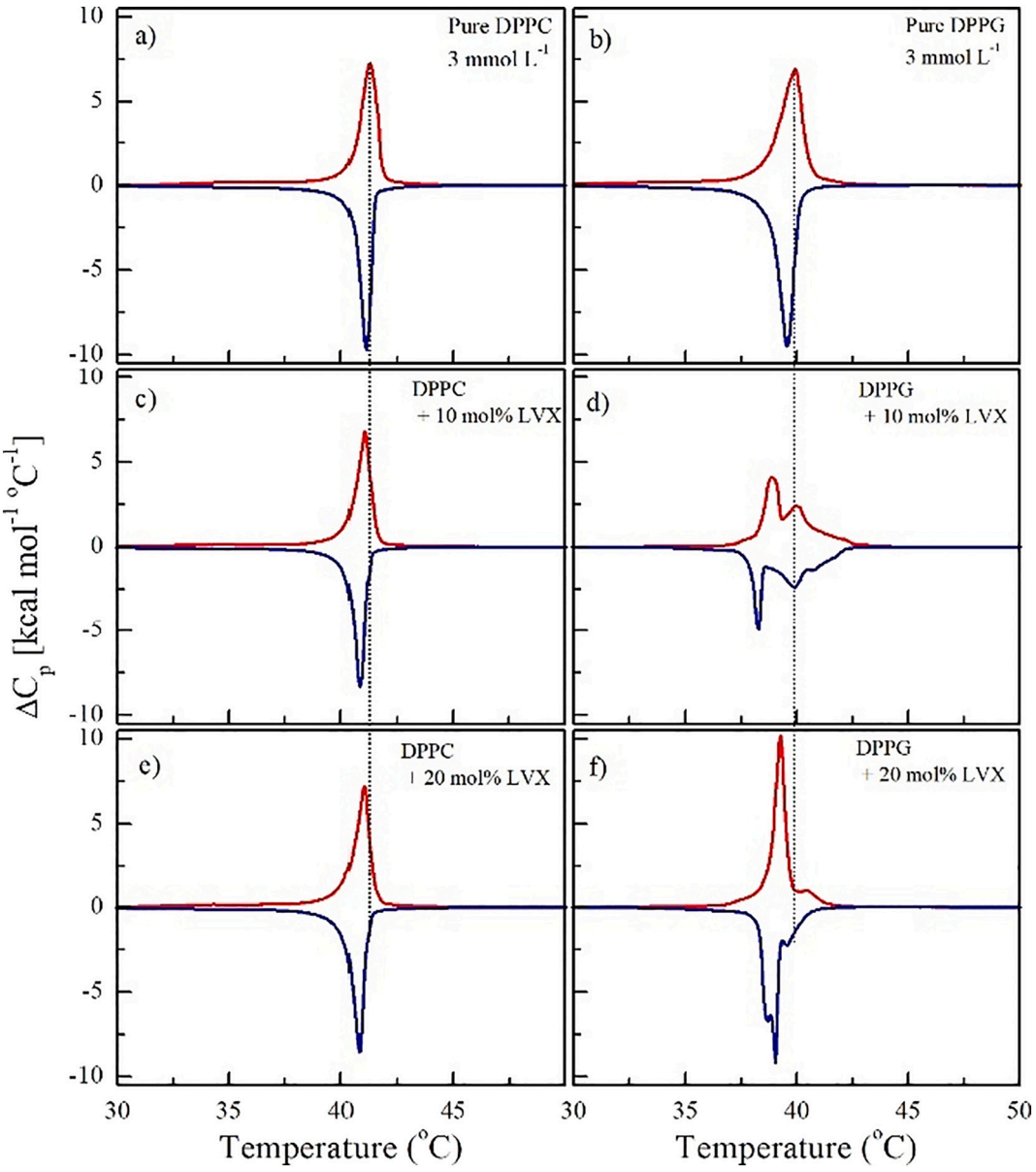

Fig. 2. Typical thermograms of 3 mmol L^{-1} DPPC (left column) and DPPG (right column) in the absence of LVX (a,b), and in the presence of increasing amounts of LVX: (c,d) 0.3 mmol L^{-1} (10 mol%), and (e,f) 0.6 mmol L^{-1} (20 mol%), under endothermic (red lines) and exothermic (blue lines) processes. The dotted lines are presented here as a visual aid to indicate the position of the maximum of the thermal peaks that correspond to pure DPPC and DPPG.

Table 1
Thermodynamic parameters for DPPC and DPPG in the absence and presence of 10 and 20 mol% LVX. *Not determined.

Lipid	%[LVX]	ΔH (kcal mol^{-1}) endothermic	ΔH (kcal mol^{-1}) exothermic	$\Delta T_{1/2}$ (°C) endothermic	$\Delta T_{1/2}$ (° C) exothermic	T_m (° C) endothermic	T_m (° C) exothermic
DPPC	0	−8.8 ± 0.2	8.5 ± 0.2	0.85 ± 0.04	0.70 ± 0.02	41.1 ± 0.2	41.0 ± 0.1
DPPC	10	−9 ± 1	9 ± 1	0.76 ± 0.08	0.6 ± 0.1	41.02 ± 0.08	40.83 ± 0.02
DPPC	20	−8.5 ± 0.3	8.4 ± 0.4	0.90 ± 0.2	0.8 ± 0.2	40.8 ± 0.4	40.8 ± 0.3
DPPG	0	−8.8 ± 0.4	8.4 ± 0.3	1.1 ± 0.1	0.76 ± 0.4	39.9 ± 0.2	39.5 ± 0.2
DPPG	10	−7.5 ± 0.3	7.5 ± 0.4	*	*	*	*
DPPG	20	−8.8 ± 0.3	8.4 ± 0.2	0.50 ± 0.09	0.7 ± 0.1	39.1 ± 0.2	39.05 ± 0.04

show a minor spontaneous leakage (less than 1%), whereas POPG liposomes (Fig. 3d) present an acceptable spontaneous leakage around 20% after 30 min, as previously reported [33]. As observed for gel liposomes, the leakage induced by 20 mol% LVX is also negligible in both fluid bilayers, POPC or POPG. Thus, CF assays show that under the experimental conditions employed in this work LVX does not induce pore formation in neither zwitterionic nor anionic liposomes, in their gel or fluid phases.

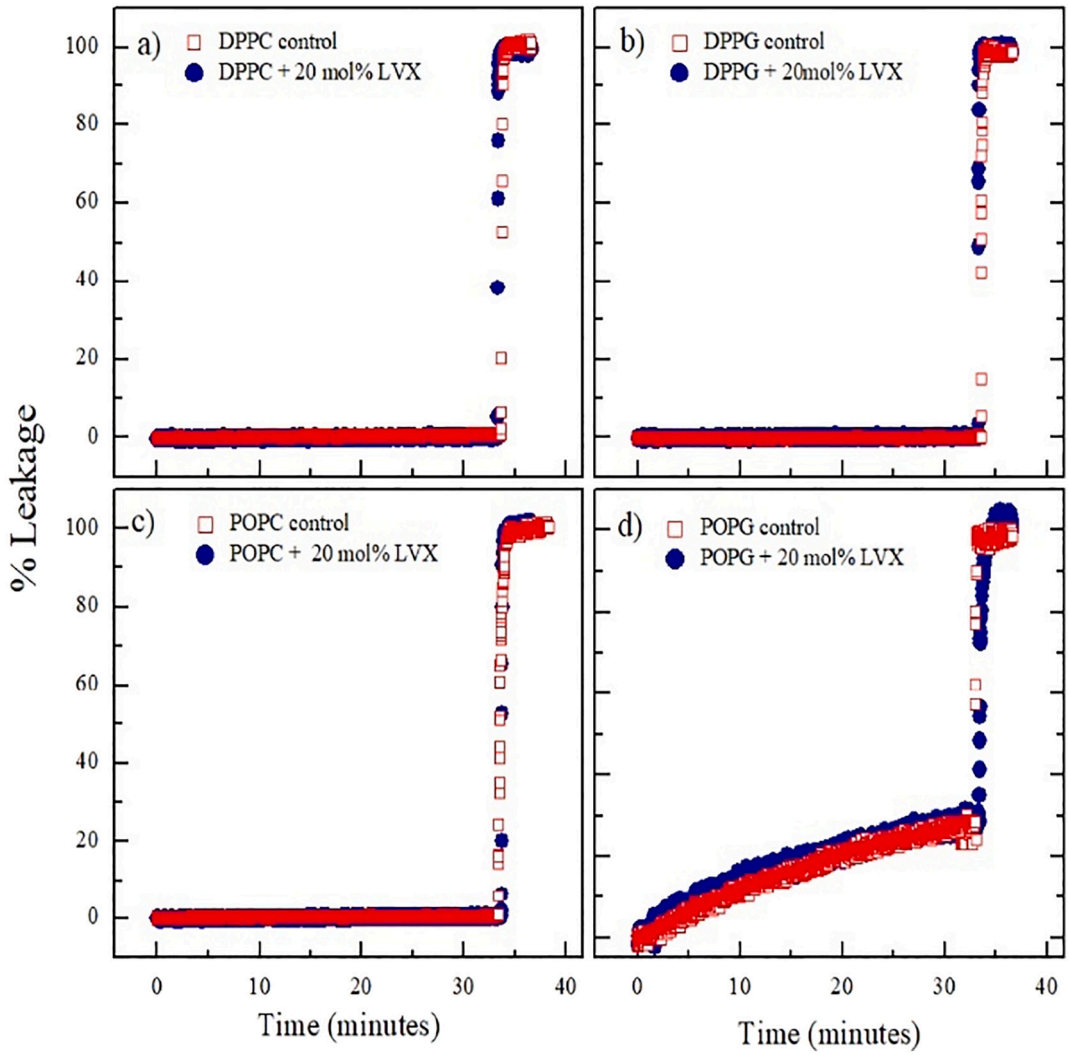

Fig. 3. Typical kinetics of CF leakage through LUVs composed of DPPC (a) and DPPG (b) in the gel phase (25 °C), POPC (c) and POPG (d) in the fluid phase (25 °C), and with the addition of 20 μmol L^{-1} LVX (blue full circle). Lipid concentration was 100 μmol L^{-1}. The control (red open square) consists of pure LUVs without the addition of the antibiotic.

3.1.3. Electron spin resonance (ESR) with spin probes

Spin label spectroscopy is a widely used technique to study amphiphilic aggregates, see, for instance [36,37]. It is a very accurate technique to probe an aggregate packing in the nano vicinity of the paramagnetic probe. In this work, we determined the rigidity/order at different levels of the ionic bilayers: at the levels of the 5th and the 16th carbon atoms of the lipid acyl chains, monitoring the region close to the polar headgroups, and the inner core of the bilayer, respectively. As exogenous molecules may interact differently with gel and fluid membranes, we studied through spin label spectroscopy the structural changes induced by LVX on the ionic bilayers at temperatures ranging from 10 °C to 60 °C, hence analyzing the gel and fluid phases of the dipalmitoyl bilayers.

3.1.3.1. ESR: LVX interaction with gel liposomes. Fig. 4 shows the ESR spectra of 5-PCSL (left column) and 16-PCSL (right column) embedded into gel unilamellar vesicles of DPPC (top three horizontal lines) and DPPG (bottom three horizontal lines), in the absence of (dark gray) and with increasing amounts of LVX: 10 mol% LVX (orange), and 20 mol% LVX (blue). The inner core of the bilayer is a region with more mobility and less order than the region closer to the polar headgroups. Accordingly, the probe 5-PCSL in DPPC (Fig. 4a) or DPPG (Fig. 4g) presents a much more anisotropic spectrum than that found for the spin label 16-PCSL incorporated into DPPC (Fig. 4d) or DPPG (Fig. 4j) membranes.

The modifications induced by the presence of LVX are not visually detected on the spin probes spectra (Fig. 4). However, they can be quantified by experimental parameters directly measured on the ESR spectra.

We plotted the maximum hyperfine splitting (A_{max}) measured on the 5-PCSL spectra versus the temperature, in the absence and in the presence of LVX (Fig. 5a,b): 10 mol% LVX (orange circle) and 20 mol% LVX (blue triangle). $2A_{max}$ provides information about the anisotropy and the speed of movement of the probe, called here the viscosity of the nano region in which the probe is incorporated. Overall, higher A_{max} values mean higher restriction to the movement of the paramagnetic probe [36]. Note that A_{max} decreases (Fig. 5a,b) as the temperature increases, showing that even in the gel phase the increase of temperature leads to a relative fluidification of the bilayer.

In Fig. 5a it is possible to observe that the presence of LVX did not induce significant changes in this parameter, with the differences smaller than the error bars, showing that LVX does not change the fluidity of gel DPPC bilayers around the 5th carbon (Fig. 5a), at least with the maximum concentration of LVX used here. In contrast, for DPPG membranes, the presence of 20 mol% LVX increases the values of A_{max} (Fig. 5b), indicating that LVX is inducing a lipid packing in the region of the 5th carbon of the acyl chain, even in the already highly

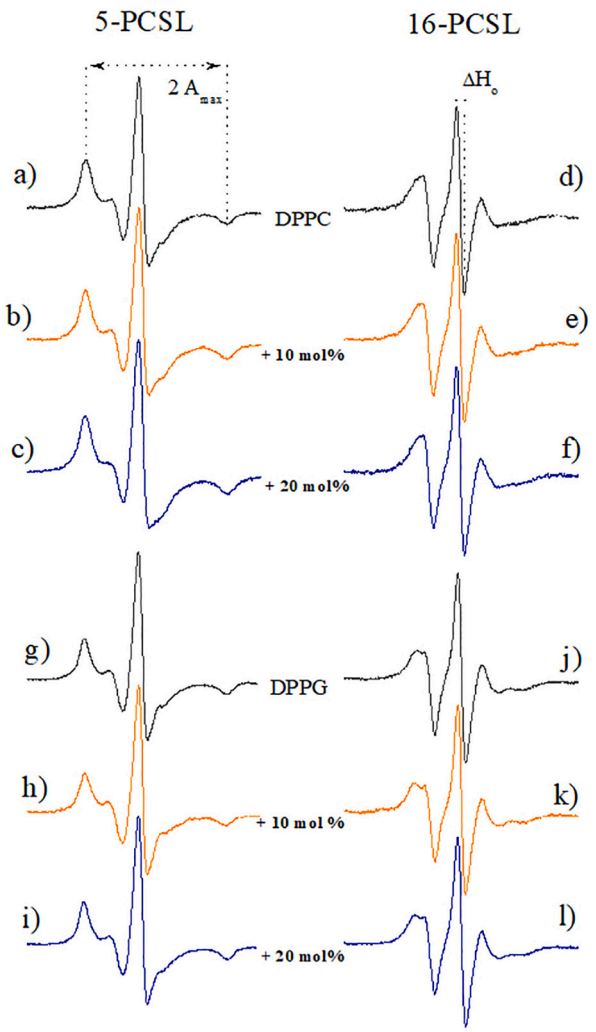

Fig. 4. Typical ESR espectra of 5-PCSL (left column) and 16-PCSL (right column) embedded into gel vesicles of DPPC (a to f) and DPPG (g to l), in the absence and presence of 10 and 20 mol% LVX. The spectra were acquired at 25 °C, corresponding to the gel phase of the lipids, and their total width is 100 G. The maximum hyperfine splitting ($2A_{max}$) and the central line width (ΔH_0) are indicated.

packed gel membrane.

ESR spectra of 16-PCSL in gel bilayers can be analyzed monitoring the central field line width (ΔH_0), thus accessing information about the restriction of molecular mobility and/or order: the higher ΔH_0, the higher the restriction of motion, hence the higher the probe anisotropy of movement [37]. Note that ΔH_0 decreases as the temperature increases (Fig. 5c,d), showing that at the bilayer core there is also an increase in the lipids mobility in the gel phase as temperature increases. Moreover, a higher packing at the bilayer core of pure zwitterionic DPPC membrane as compared to that of pure DPPG anionic membrane is observed, since higher values of ΔH_0 are measured for pure DPPC Fig. 5(c,d). This is probably due to the electrical repulsion between the anionic polar headgroups of DPPG, making the bilayer more fluid at its core.

The effects of LVX on the core of gel liposomes of DPPC and DPPG are similar to those found at the region close to the 5th carbon atom. LVX does not induce any significant change in the inner core of DPPC bilayers, as can be attested by Fig. 5c. In contrast, LVX strongly modifies the core of DPPG bilayer, as shown by the changes in ΔH_0 values (Fig. 5d). For lower temperatures, 10 °C and 15 °C, the presence of 10 and 20 mol% of LVX increases the values of ΔH_0 measured on the 16-PCSL spectra, hence increases the packing of the bilayer at its core. At 20 °C, only 20 mol% of LVX alter the packing of DPPG membranes, and no effect of the drug was detected for higher temperatures.

3.1.3.2. ESR: LVX interaction with fluid liposomes. In Fig. 6, we see the ESR spectra of 5-PCSL (left column) and 16-PCSL (right column) embedded into 3 mmol L^{-1} fluid liposomes of DPPC (top three horizontal lines) and DPPG (bottom three horizontal lines) in the absence of (dark gray) and with increasing amounts of LVX: 10 mol% LVX (orange), and 20 mol% LVX (blue).

Once again, the effects of LVX are not visually evident on the spectra but can be accessed through experimental parameters directly measured on the ESR spectra. For fluid membranes, we can evaluate the impact of the antibiotic in the vicinity of the 5th carbon of the paraffinic chain by calculating the effective order parameter (S_{eff}) (see Section 2.5). As discussed in [37], values of S_{eff} close to the unity indicate that the bilayer region monitored by the spin probe is highly anisotropic. In opposition to that, S_{eff} values tend to zero when the probe is in rapid and isotropic movement, indicating a quite loose nano-environment. Thus, S_{eff} provides information about the organization/mobility of the lipid bilayer at the level of the 5th carbon atom.

The values of S_{eff}, are smaller for DPPG (Fig. 7b) membranes than for DPPC (Fig. 7a), showing that, in the fluid phase, zwitterionic membranes present a higher packing and/or order than anionic liposomes even around the 5th carbon atom position. Similar to the results found for the gel bilayers, the presence of LVX in fluid membranes of DPPC (Fig. 7a) does not have any significant impact on the organization of the bilayer, as indicated by the constancy of S_{eff}. For anionic membranes of DPPG, 20 mol% LVX induced a significant increase in S_{eff} values indicating that LVX also increases the packing of fluid DPPG bilayers.

For the ESR spectra of 16-PCSL, in fluid membranes, the amplitude of the three hyperfine lines, corresponding to $m_1 = +1, 0, -1$, can be directly measured on the ESR spectra (Fig. 6, right column). The ratio between the amplitudes of the lines, (h_{-1}/h_o), is an empirical parameter related to the packing of the bilayer: h_{-1}/h_o tends to unity as the probe movement becomes less ordered and faster [32]. This parameter shows that the core of fluid DPPC bilayers is also a region of more restriction of mobility than that of DPPG, since the values of h_{-1}/h_o are smaller for DPPC (Fig. 7c) than for DPPG (Fig. 7d) membranes. Once more, the presence of LVX almost does not have any impact on the mobility and/or packing of the core of fluid DPPC bilayers, since the values of h_{-1}/h_o are the same within the error bars (Fig. 7c). In opposition to that, the values of h_{-1}/h_o measured at different temperatures are smaller in the presence of 10 mol% and 20 mol% LVX than those found for pure DPPG vesicles (Fig. 7d). This makes evident that in those concentrations LVX increases the lipid packing at the core of DPPG bilayers. It is interesting that 10 mol% LVX did not induce changes in S_{eff} (Fig. 7b), whereas increases the values of h_{-1}/h_o. That could be due to the sensitivity of the paramagnetic probes. As 5-PCSL is located in a region with more restriction of mobility than that at the core of the bilayer, 16-PCSL is usually more sensitive to changes in the nano-environment viscosity than 5-PCSL.

3.2. Modifications induced in LVX by the presence of ionic membranes: intrinsic LVX fluorescence emission

In the previous sections, by using DSC, CF assay, and spin label spectroscopy, we monitored the membranes, and the changes induced on these membranes due to the presence of LVX. Like many of the FQ molecules, LVX is fluorescent. Here, we exploit this property to investigate the changes induced on LVX by increasing concentrations of membranes, both zwitterionic and anionic LUVs, thus having a more complete picture of the interaction of LVX with ionic bilayers.

3.2.1. Stead-state fluorescence spectroscopy

Depending on the lipid concentration, the light scattering can be too strong, usually more intense for zwitterionic than for anionic

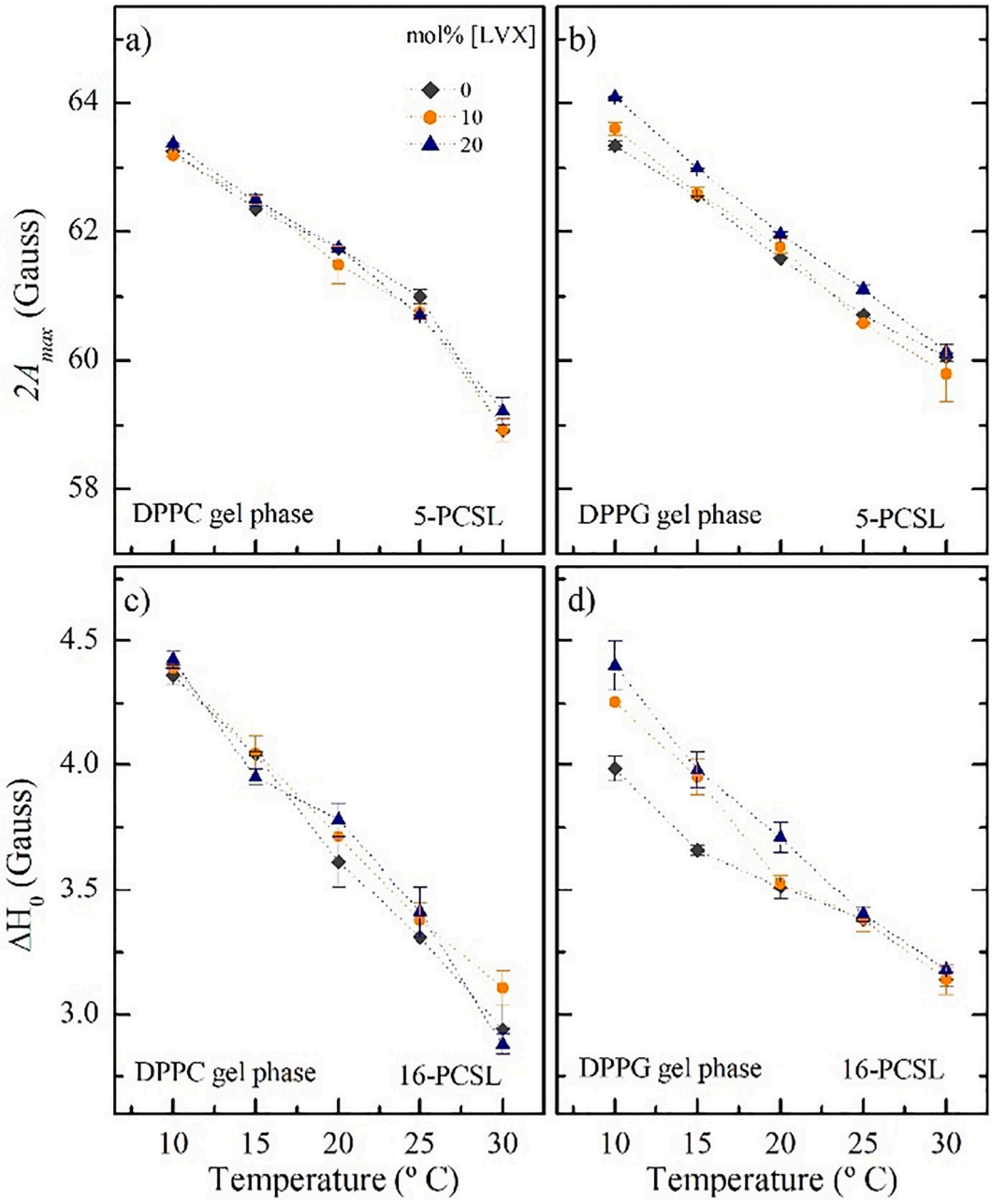

Fig. 5. Temperature dependence of the outer hyperfine splitting ($2A_{max}$) measured on the ESR spectrum of 5-PSCL embedded into 3 mmol L^{-1} gel liposomes of DPPC (a) and DPPG (b). Temperature dependence of the central field line width (ΔH_0) measured on the ESR spectrum of 16-PCSL embedded into 3 mmol L^{-1} gel liposomes of DPPC (c) and DPPG (d). The data were obtained in the absence of LVX (dark gray diamond), in the presence of 10 mol% LVX (orange circle), and 20 mol% LVX (blue triangle). Error bar indicates standard deviation of at least three experiments with different samples. If not shown, the deviation was found to be smaller than the symbol.

membranes. Particularly, the light scattering yielded by DPPC gel vesicles is too strong (Fig. SM1) for reliable inner filter corrections (see Eq. (3)). Therefore, for zwitterionic membranes, we only exhibit the fluorescence spectra of LVX in the absence and with increasing amounts of fluid (50 °C) zwitterionic vesicles of DPPC (Fig. 8a). As the light scattering for anionic vesicles is significant lower, we show the LVX emission spectra with increasing concentrations of gel (25 °C, Fig. 8b) and fluid (50 °C, Fig. 8c) DPPG vesicles.

The fluorescence spectrum of LVX at physiological pH is in good agreement with that reported in the literature, with a maximum emission peak at 457 nm [45,46]. The presence of zwitterionic DPPC vesicles does not alter the LVX spectrum (Fig. 8a). Contrary to that, increasing amounts of anionic DPPG vesicles shift the LVX emission spectrum to longer wavelengths (lower energies) (Fig. 8b,c), showing that LVX interacts with both gel and fluid DPPG membranes. At the maximum lipid concentration used here, 10 mmol L^{-1} DPPG, maximum redshifts of 19 nm and 29 nm (Fig. 8d) for gel and fluid membranes are observed, respectively.

3.2.2. *Time-resolved (TR) fluorescence spectroscopy*

Time-resolved fluorescence spectroscopy is a good approach to study molecules when light scattering is significantly high, since fluorescent lifetimes have little dependence on the fluorophore emission intensity [38,47]. Hence, we measured the fluorescence decay of LVX in the absence of lipid vesicles, and with increasing concentrations of gel vesicles (25 °C) of DPPC (Fig. 9a) and DPPG (Fig. 9b), and fluid vesicles

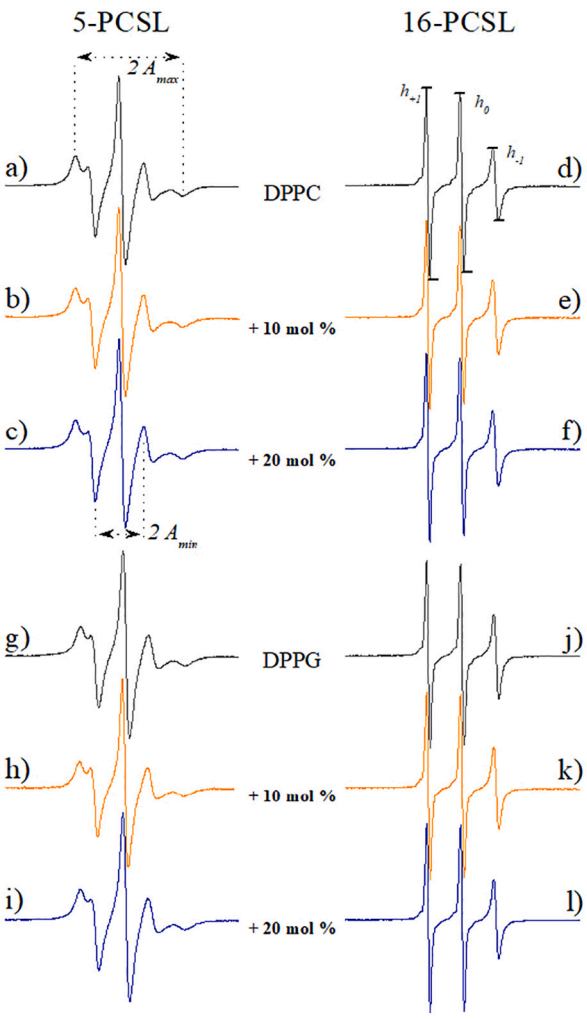

Fig. 6. Typical ESR espectra of 5-PCSL (left column) and 16-PCSL (right column) embedded into fluid vesicles of DPPC (a to f) and DPPG (g to l), in the absence and presence of 10 and 20 mol% LVX. The spectra were acquired at 50 °C, corresponding to the fluid phase of the lipids, and their total width is 100 G. The maximum and minimum hyperfine splitting ($2A_{max}$ and $2A_{min}$, respectively), and the amplitudes of the low (h_{+1}), central (h_o) and high (h_{-1}) fields are indicated.

(50 °C) of DPPC (Fig. 9c) and DPPG (Fig. 9d).

In buffer, at 25 °C and 50 °C, the excited state decay curves of LVX were well fitted by monoexponential decays (see Eq. (4)) yielding lifetimes equal to (6.30 ± 0.01) ns and (5.04 ± 0.01) ns, respectively. As expected, the lifetime at 50 °C is smaller in comparison with that found at 25 °C. This is due to the increase of non-radiative decay processes as temperature increases [38]. The decay curves of LVX in the presence of gel (Fig. 9a) or fluid (Fig. 9c) DPPC vesicles do not present any significant changes with respect to pure LVX decay curves: no change is observed in the angular coefficient of the lines in the semi-log plot shown in Fig. 9a and c. Accordingly, the lifetimes found from the best fittings (Eq. (4)) of the decay curves of LVX in the presence of increasing amounts of DPPC do not change much, as evinced in Fig. SM2. This is a strong indication that LVX, at physiological pH, has little affinity to zwitterionic DPPC liposomes.

In contrast, the LVX decay curves in the presence of anionic vesicles of DPPG (Fig. 9b,d) radically change. They cannot be fitted with just one exponential (Eq. (4)), as for LVX in buffer or in the presence of DPPC vesicles. To fit the curves in the presence of gel and fluid DPPG vesicles (Fig. 9b,d), according to the statistical criterium ($0.95 \leq \chi^2 \leq 1.3$), two terms were necessary in Eq. (4), indicating the presence of at least two lifetimes. Hence, we used a global analysis to evaluate all the LVX decay curves at a given temperature, in the presence of different DPPG concentrations. Accordingly, we made the hypothesis that all the decaying curves obtained at a given temperature, from samples with different lipid concentrations, were a composition of decaying processes coming from two different species only: one in aqueous environment and one in the lipid phase. Hence, this method consisted in fitting all the decay curves with two lifetimes only, namely LVX lifetime in aqueous environment (τ_1) and LVX lifetime in the lipid phase (τ_2). For each temperature, the decay curve was fitted with a different fractional contribution of the two lifetimes, f_1 and f_2, corresponding to the contributions of the lifetimes relative to LVX in the aqueous and lipid phase, respectively.

The global analysis for the curves in the presence of gel (25 °C) DPPG vesicles (Fig. 9b) yielded a lifetime for LVX in buffer of $\tau_1 = 6.26$ ns, and a lifetime for LVX in the lipid gel phase, $\tau_2 = 12.55$ ns ($\chi^2 = 1.22$). Table SM1 displays the result of the global analysis for each decay curve in the presence of gel (25 °C) DPPG vesicles. For the decay curves at 50 °C (Fig. 9d), the global analysis yielded a lifetime in buffer of $\tau_1 = 5.01$ ns and$\tau_2 = 9.70$ ns. The results of the global analysis for each decay curve at 50 °C is available in Table SM3. In addition, Figs. SM3 and SM4 display the fittings and the weighted residuals from the global analysis for LVX decay curves in the presence of gel and fluid DPPG liposomes, respectively.

Considering that all curves obtained at a given temperature, in the presence of different amounts of lipid, could be well fitted by just two lifetimes, one of them (τ_1) being very similar to the value found for LVX in buffer, the hypothesis mentioned above seemed quite robust. Moreover, the lifetimes in the lipid phase, τ_2, were found to be higher than those found for LVX in buffer, τ_1. This is probably due to the decrease of non-radiative relaxation processes, either related to decrease in the interaction between LVX and solvent molecules, and/or related to restrictions on LVX motion.

Therefore, Fig. 10 displays the fractional contribution of LVX lifetime in the lipid phase (f_2) as the concentration of DPPG increases, for lipids in the gel (25 °C) and fluid (50 °C) phases. The experimental data, at both temperatures, could be well fitted by a conventional binding isotherm (Eq. (5)), yielding apparent LVX-lipid partition constants (K_p) for DPPG gel and fluid phases.

We estimated $\gamma_L = 0.67$ L mol^{-1} and 0.71 L mol^{-1}, for gel and fluid DPPG membranes (Eq. (5)), respectively, from data in the literature [24]. The parameters from the best non-linear fitting processes are displayed in Table 2.

Interesting to note that K_p was found to be higher for the fluid DPPG phase, as compared with the gel lipid phase (Table 2). This is in accord with the results obtained with steady-state fluorescence (Fig. 8), which showed a larger red-shift for LVX in the presence of fluid DPPG membranes.

4. Discussion

Different techniques were employed to characterize the interaction of the antibiotic levofloxacin with zwitterionic and anionic membranes. That was performed having in mind one of the main differences between mammalian and prokaryotic membrane cells: the latter display anionic lipids in its outer membrane [24].

Studying structural alterations on the membranes, with DSC, spin labels incorporated in the bilayers, and monitoring bilayer pores formation with the fluorescent probe CF, we found no effect of LVX on DPPC membranes, up to the concentration of 20 mol% of LVX relative to the lipid. Similarly, monitoring the LVX fluorescence, we found no change produced by DPPC on the molecule emission properties. Hence, we detected no interaction between LVX and DPPC membranes.

Opposite to that, all the employed techniques showed that LVX interacts with anionic DPPG vesicles. Fluorescence properties of the antibiotic are severely altered in DPPG dispersions, and the antibiotic

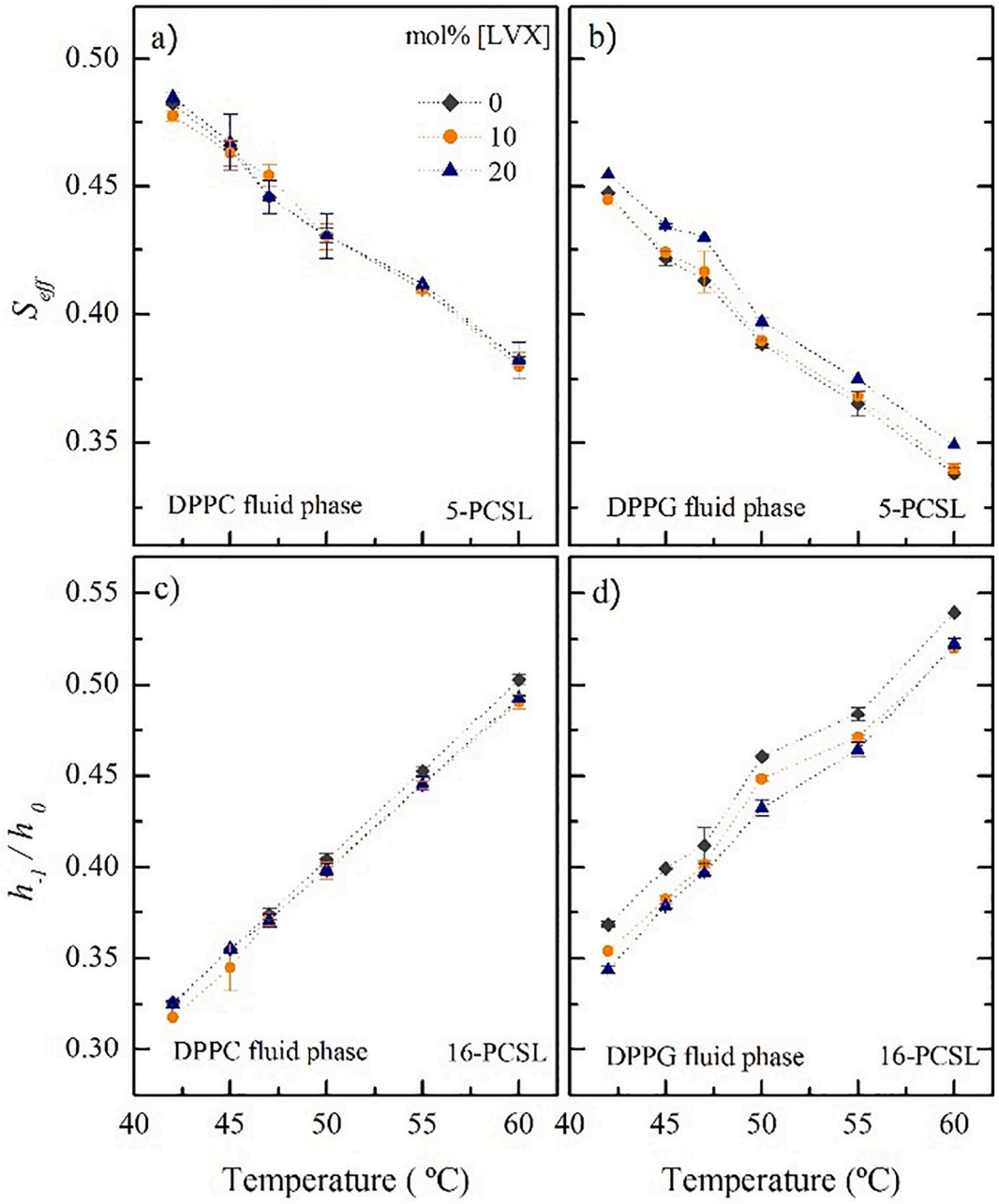

Fig. 7. Temperature dependence of the effective order parameter, S_{eff}, measured on ESR spectra of 5-PCSL incorporated into 3 mmol L^{-1} of fluid liposomes of DPPC (a) and DPPG (b). Temperature dependence of the ratio of the low and central field line amplitudes, h_{-1}/h_o, measured on the ESR spectrum of 16-PCSL embedded into 3 mmol L^{-1} of fluid membranes of DPPC (c) and DPPG (d). The data were obtained in the absence of LVX (dark gray diamond), and in the presence of 10 mol% LVX (orange circle), and 20 mol% LVX (blue triangle). Error bar indicates standard deviation of at least three experiments with different samples. If not shown, the deviation was found to be smaller than the symbol.

changes the DPPG bilayer structure. Important to point out that we worked at physiological pH, 7.4, where LVX is supposed to be mostly zwitterionic (see Fig. 1).

The presence of 10 mol% LVX drastically changed DPPG thermotropic behavior (Fig. 2, right column). The well-defined one peak of the DPPG gel-fluid transition, monitored by DSC, was turned into two peaks. One of them corresponding to bulk DPPG and the other one related to LVX-bound lipids. Upon increasing the LVX concentration to 20 mol%, just the LVX-bound thermal peak is detected, indicating that DPPG membranes are saturated with the antibiotic, thus the peak corresponding to free lipids is no longer detectable. Hence, the interaction LVX-DPPG would be strong enough to create LVX-rich domains in DPPG membranes, for lower antibiotic concentrations. That has been observed before with the interaction of cationic molecules with anionic lipids (see, for instance, Ref. [33, 48]), and has been attributed to a strong ionic interaction between the exogenous molecule and the lipid bilayer.

To further investigate the relevance of the negative charge of DPPG on its interaction with LVX, we performed experiments with extruded DPPG dispersions at high ionic strength conditions (10 mmol L^{-1} HEPES, 250 mmol L^{-1} NaCl, pH 7.4), where it is expected that most of the DPPG headgroups would be neutralized by Na^+ ions. Only minor differences were detected on the DPPG thermograms by the addition of up to 20 mol% LVX (Fig. SM4 and Table SM3). Similarly, LVX fluorescent properties did not change in the presence of high ionic strength DPPG dispersions (Fig. SM5). These findings strongly sustain our hypothesis that the electrostatic interaction plays a key role on the LVX-

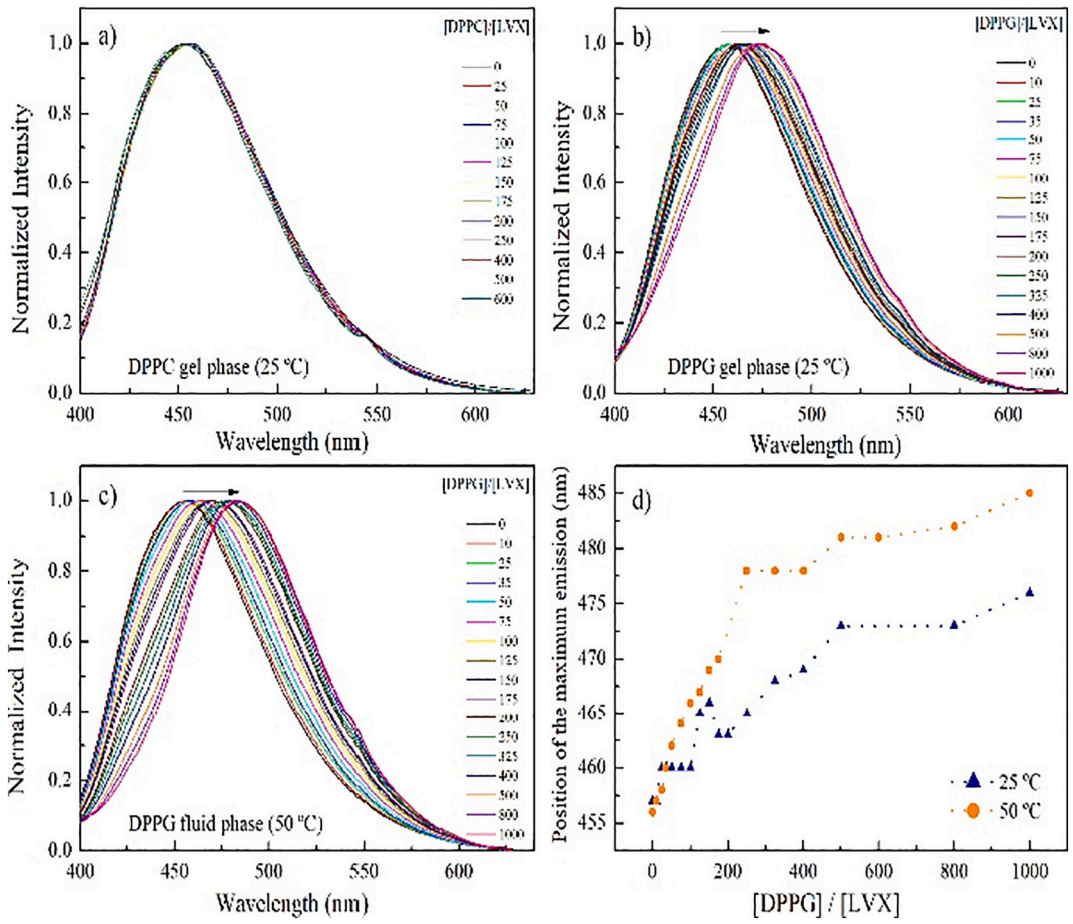

Fig. 8. Normalized fluorescence spectra of LVX in buffer (in the absence and in the presence of increasing relative concentrations of fluid (50 °C) vesicles of DPPC (a), and gel (b) and fluid (c) DPPG. The arrows in figures b) and c) are aid for the eyes and indicate the increasing of DPPG concentration. (d) Position of the maximum emission as a function of the relative concentration of gel (25 °C, blue triangle) and fluid (50 °C, orange circle) [DPPG]/[LVX] concentration. The dotted lines are only guide for the eyes. [LVX] = 0.01 mmol L^{-1}. Excitation light beam at 345 nm.

membrane binding.

It is interesting to observe that the presence of LVX induces an increase on the cooperativity of the gel-fluid transition of DPPG bilayers, with $(\Delta T_{1/2})$ decreasing from (1.1 ± 0.1) °C to (0.50 ± 0.09) °C, the latter in the presence of 20 mol% LVX. Hence, the presence of LVX seems to increase the lipid-lipid interaction. That is opposite to the effect observed, for instance, when the cationic peptide K^0-W^6-Hya1 binds to DPPG membranes, inducing peptide-bound domains: a broadening of the gel-fluid transition is observed, indicating a decrease on lipid-lipid interaction [33]. This result is in accord with the peptide deeply penetrating into the lipid bilayer, as indicated by the alterations on the fluorescence of the Trp residue present in K^0-W^6-Hya1.

It is also important to point out that LVX interacts with DPPG membranes, altering their gel-fluid thermogram, creating LVX-lipid rich domains in DPPG membranes, but the antibiotic does not induce pore formation on the membrane (Fig. 3), as the cationic peptide K^0-W^6-Hya1 mentioned above was found to do [33].

As multilamellar vesicles display a narrower gel-fluid transition as compared with unilamellar structures, we had to investigate whether LVX would be inducing the presence of DPPG multibilayer vesicles. An experiment was performed that indicated no rearrangement of DPPG LUVs in the presence of LVX, as follows. Spin labels incorporated in fluid DPPG vesicles can be used to indicate fusion or coalescence of vesicles in an aqueous dispersion, through the measurement of the spin-spin interaction [49,50]. An excess of spin labels in a membrane can be clearly detected by the broadening of the ESR spectrum due to spin exchange. Accordingly, at the lipid fluid phase (60 °C), 0.3 mmol L^{-1} of DPPG labeled with an excess of 16-PCSL (3 mol%) clearly displays a broad ESR spectrum, typical of spin-spin interaction (Fig. SM7). This broad ESR signal was found to be unchanged by the addition of unlabeled DPPG dispersion (2.7 mmol L^{-1}), in the absence and in the presence of 20 mol% LVX, (Fig. SM7). That is a strong evidence that there is no coalescence of vesicles, which would lead to a narrower ESR spectrum, due to the fusion of spin-labeled and unlabeled DPPG vesicles, reducing the spin label concentration on the bilayer, hence reducing the spin-spin interaction [51].

It was interesting to find that the ESR spectra of spin labels, both at the 5th and at the 16th atom of the hydrocarbon chain, show that the binding of LVX to DPPG membranes increases the packing of the bilayer, both at the gel and at the fluid membrane phases (Figs. 5 and 7). That is another indication that LVX is not penetrating the DPPG bilayer core, and strongly disrupting its structure, but somehow staying close to the bilayer surface, interacting with the anionic PG headgroups, shielding the PG^--PG^- repulsive interaction, hence allowing the DPPG bilayer to get more packed, increasing lipid-lipid interaction. That would explain the presence of a somewhat more cooperative gel-fluid transition in the presence of 20 mol% LVX, monitored by DSC, as discussed above.

The localization of LVX on DPPG membranes can be also assessed by the effect the membrane causes on the fluorescence properties of LVX. In general, when a fluorophore penetrates a lipid bilayer, a more hydrophobic environment, its emission spectrum shifts to smaller wavelengths (higher energies), in comparison with the spectrum of the fluorophore in aqueous environment, as the fluorophore dipolar relaxation with the solvent decreases considerably in the lipid phase [40]. But the reverse

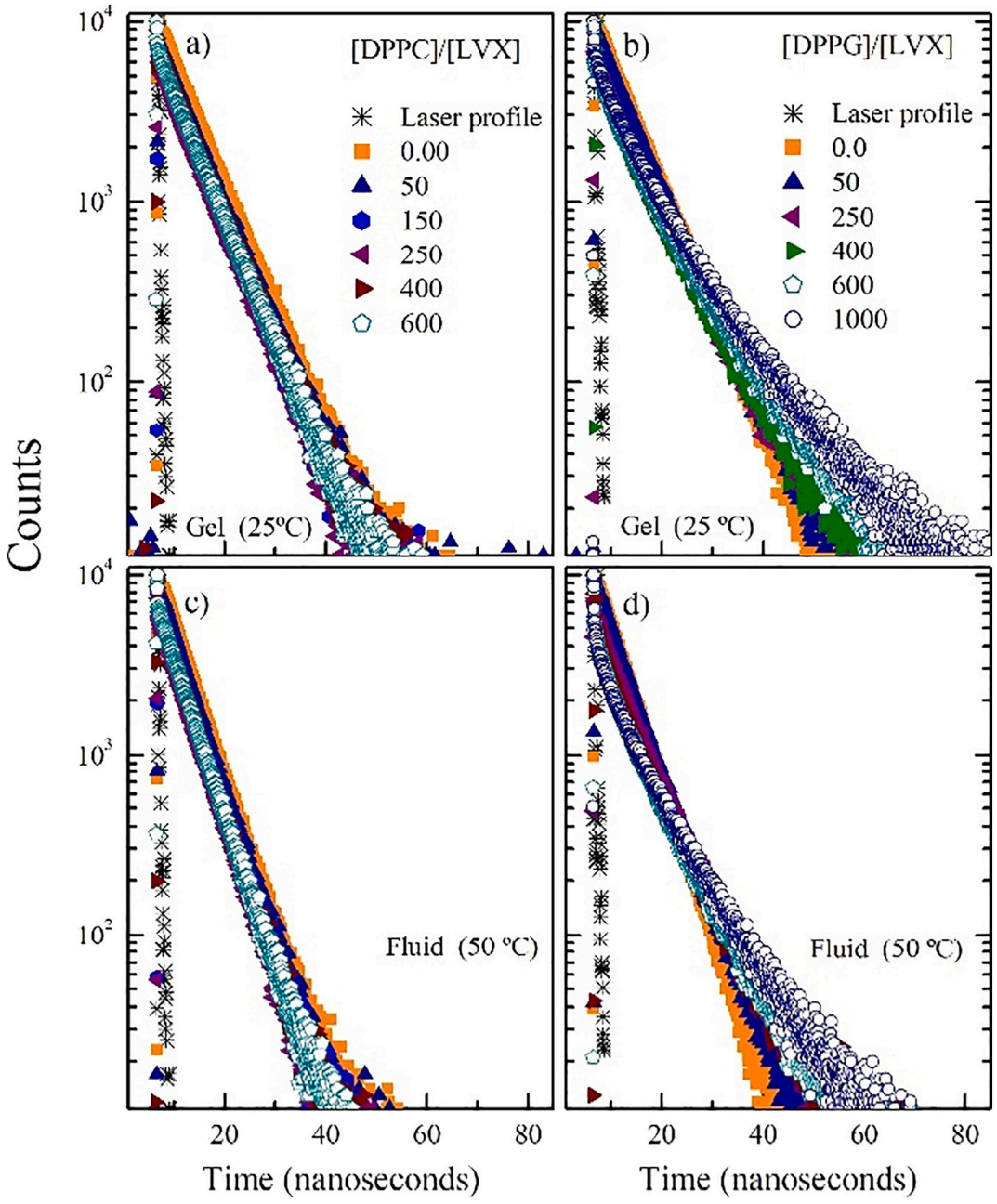

Fig. 9. Typical fluorescence decay curves of LVX in the absence and in the presence of increasing concentrations of lipids: gel vesicles (25 °C) of DPPC (a) and DPPG (b), and fluid vesicles (50 °C) of DPPC (c) and DPPG (d). Excitation beam light at 284 nm and emission fluorescence at 457 nm. [LVX] = 0.01 mmol L^{-1}.

was observed with the emission spectrum of LVX in the presence of DPPG membranes: a large redshift was observed, being 19 nm and 29 nm, for gel (25 °C) and fluid (50 °C) DPPG phases, respectively, for the maximum lipid concentration used here.

However, time resolved fluorescence detected a significant increase on the lifetime of the excited state of LVX in the presence of DPPG: at 25 °C (gel membrane), it went from $\tau_1 = 6.26$ ns in buffer to $\tau_2 = 12.55$ ns in DPPG, and at 50 °C (fluid membrane), it went from $\tau_1 = 5.01$ ns in buffer to $\tau_2 = 9.70$ ns in DPPG. A longer lifetime is expected for a fluorophore inserted in a lipid membrane in comparison to the molecule in a water medium, due to the reduction in non-radiative deactivation processes related with interactions with solvent molecules and/or a restriction on molecular mobility, the latter due to the increase on the viscosity at the fluorophore's vicinity [38].

The apparent contradiction between the results obtained with steady-state and time-resolved fluorescence can be rationalized if we consider that the fluorescence emission of LVX is extremely dependent on the pH value of the medium, the maximum of the emission band moving from 457 nm to 498 nm, as the solution pH goes from 7.0 to 4.5. As can be seen in Fig. 11, the emission band of LVX in the presence of the maximum concentration of DPPG used here, in buffer at pH 7.4, is in between the bands obtained for the antibiotic in aqueous solutions at pH values 6.0 and 5.5, with a maximum emission at 486 nm. Therefore, the observed red shift of the LVX fluorescence band in the presence of DPPG vesicles (Fig. 6) is most likely indicating that the antibiotic protonates close to the DPPG membrane. LVX protonation would be expected due to the lower local pH close to the anionic PG^- membrane [52,53]. Indeed, the protonation of some FQs under binding anionic amphiphilic aggregates, and anionic domains in protein, have been previously reported [17,54–56].

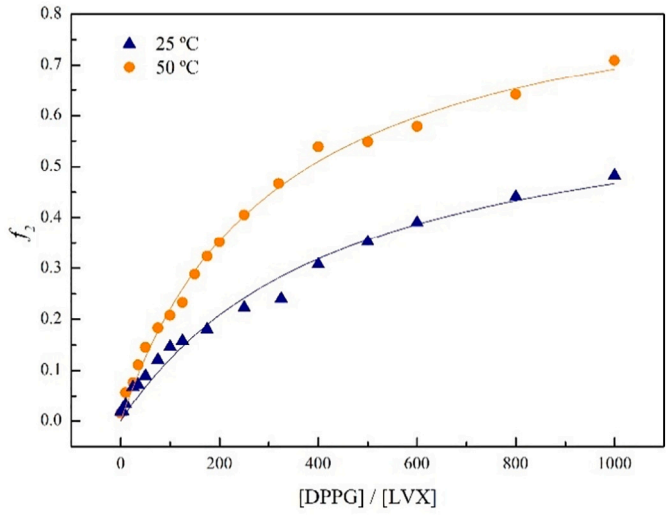

Fig. 10. Fractional contribution of LVX lifetime in the lipid phase (f_2, Eq. (4)): corresponds to gel (25 °C, blue triangle) and fluid (50 °C, orange circle) DPPG phases. The data are from four independent experiments. The lines correspond to the fittings according to Eq. (5).

Table 2
Apparent partition constants of LVX in gel (25 °C) and fluid (50 °C) DPPG membranes (K_p), and the fit goodness metric (χ^2) (Eq. (5) and Fig. 10).

Temperature (°C)	K_p	χ^2
25	$(3.3 \pm 0.5) \times 10^2$	0.98
50	$(4.5 \pm 0.3) \times 10^2$	0.99

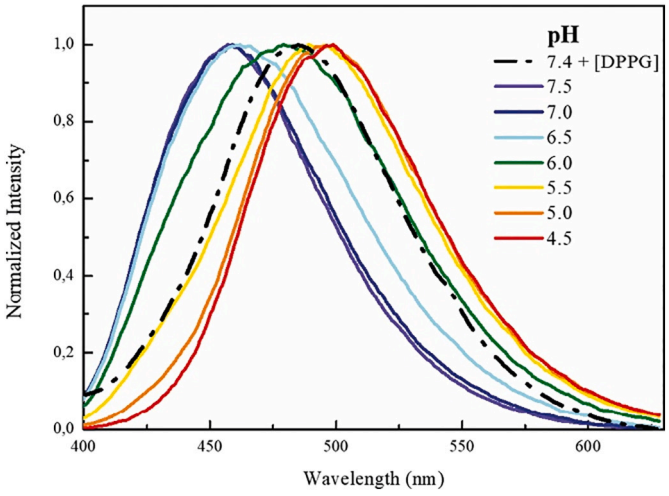

Fig. 11. Normalized emission spectra of 0.01 mmol L^{-1} LVX in universal buffer, at different pH values, and 0.01 mmol L^{-1} LVX (10 mmol L^{-1} HEPES, 3 mmol L^{-1}, pH 7.4) in extruded DPPG dispersion (10 mmol L^{-1}). Temperature = 50 °C.

Accordingly, the protonation of LVX would render the molecule cationic (see Fig. 1), which would explain its strong binding to DPPG membranes, giving rise to rich-LVX domains in the membrane, as monitored by DSC (see Fig. 2). Parallel to that, we know that part of the molecule penetrates the membrane, as an increase in the lifetime of the LVX excited state is monitored in the presence of DPPG, and LVX excited state lifetime in solution was found to be very similar at different pH values, from 7.5 to 4.5 (The antibiotic is not fluorescent at higher pH values).

Hence, the LVX fluorescence spectrum in DPPG dispersion, would be a result of two effects: LVX transition from zwitterionic to cationic species and its partial penetration into the membrane. Moreover, not all LVX molecules are bound to the membrane, since f_2 value does not reach 1 under the maximum DPPG concentration used here, 10 mmol L^{-1} (Fig. 10). For instance, at this DPPG concentration with fluid vesicles, there is still about 30% LVX in the aqueous phase.

Taken together, we would like to suggest that LVX when bound to DPPG membrane is mostly in its cationic structure (Fig. 1), with the protonated amine group of the piperazine ring strongly bound to negative phosphate groups at the bilayer surface. However, due to the neutralization of the carboxylic group, the fluorescent moiety of the quinolone ring would penetrate the DPPG membrane, but not very deep.

There is a strong electrostatic binding between protonated LVX to PG^- at the membrane level, with partial penetration of the antibiotic into the membrane. The partition constant was found to be $(4.5 \pm 0.3) \times 10^2$ and $(3.3 \pm 0.5) \times 10^2$, for gel and fluid membranes, respectively (Table 2). That means that when we have 20 mol% of LVX in 3 mmol L^{-1} of DPPG, the actual percentage of bound LVX on the membrane is around 8 mol% of LVX with respect to the total lipid concentration. So, that is the concentration of bound LVX that induces the observed thermotropic changes in DPPG bilayers (Fig. 2f) and rigidifies both the gel (Fig. 5b and d) and fluid (Fig. 7b and d) phases of DPPG bilayers.

5. Conclusions

Though LVX and some other FQs have been reported to interact with zwitterionic membranes at physiological pH [21,23], under the conditions used here, we found no indication of the interaction between LVX and zwitterionic DPPC vesicles.

LVX binds strongly to DPPG membrane, possibly at its surface, inducing LVX-bound domains coexisting with pure lipid domains, but the antibiotic does not induce pore formation on the bilayer. Fluorescence experiments strongly suggest that LVX protonates at the DPPG membrane surface, possibly due to its lower local pH value, making the LVX-membrane binding a strong ionic interaction (see Fig. 1). The neutralization of the LVX carboxyl group would allow the quinolone ring to insert into the DPPG membrane, whereas the LVX piperazine cationic distal amine would attach to PG groups.

At the highest LVX/DPPG relative concentration used here, 20 mol%, thermograms reveal a remarkable increase in the DPPG melting/fusion cooperativity, which are associated with the increase in the packing of the bilayer, the latter monitored by spin labels incorporated in the membrane.

Given that healthy mammalian cells display zwitterionic lipids in their outer membrane leaflet, whereas bacteria are known to display anionic lipids in their membranes, a better understanding of the interaction of FQs with different lipids can provide important information of pharmacological relevance. Hence, we consider important to further investigate the interaction of different FQs with model membranes, under the same conditions, relating the results with their structural properties, with the goal of unravelling their differences concerning bioavailability, toxicity, and performance against microorganisms.

CRediT authorship contribution statement

Gabriel S. Vignoli Muniz: Conceptualization, investigation, data analysis, writing-original draft, reviewing. **Mariana C. Souza**: Investigation, data analysis. **Evandro L. Duarte**: Investigation, data analysis, conceptualization. ***M. Teresa* Lamy**: Supervision, writing, reviewing.

Declaration of competing interest

The authors declare that they have no known competing financial interests or personal relationships that could have appeared to influence the work reported in this paper.

Data availability

No data was used for the research described in the article.

Acknowledgment

This work was supported by the Brazilian agencies CNPq and FAPESP (2017/25930-1). M.T.L. is recipient of a CNPq research fellowships. G.S.V.M., E.L.D. and M.T.L. acknowledge support from the National Institute of Science and Technology Complex Fluids (INCT-FCx), financed by CNPq (141260/2017-3) and FAPESP (2014/50983-3 and 2018/20162-9). The authors are pleased to thank Dr. Sonia R. W. Louro for important discussions.

Appendix A. Supplementary data

Supplementary data to this article can be found online at https://doi.org/10.1016/j.bbamem.2021.183622.

References

[1] D.S. North, D.N. Fish, J.J. Redington, Levofloxacin, a second-generation fluoroquinolone, Pharmacotherapy. 18 (1998) 915–935, https://doi.org/10.1002/j.1875-9114.1998.tb03925.x.
[2] T.D.M. Pham, Z.M. Ziora, M.A.T. Blaskovich, Quinolone antibiotics, MedChemComm. 10 (2019) 1719–1739, https://doi.org/10.1039/C9MD00120D.
[3] L. Mandell, G. Tillotson, Safety of fluoroquinolones: an update, Can. J. Infect. Dis. 13 (2002) 54–61, https://doi.org/10.1155/2002/864789.
[4] P. Bhattacharya, S. Mukherjee, S.M. Mandal, Fluoroquinolone antibiotics show genotoxic effect through DNA-binding and oxidative damage, Spectrochim. Acta A Mol. Biomol. Spectrosc. 227 (2020) 117634, https://doi.org/10.1016/j.saa.2019.117634.
[5] L. Strekowski, B. Wilson, Noncovalent interactions with DNA: an overview, Mutat. Res. Mol. Mech. Mutagen. 623 (2007) 3–13, https://doi.org/10.1016/j.mrfmmm.2007.03.008.
[6] T. Mach, P. Neves, E. Spiga, H. Weingart, M. Winterhalter, P. Ruggerone, M. Ceccarelli, P. Gameiro, Facilitated permeation of antibiotics across membrane channels – interaction of the quinolone moxifloxacin with the OmpF channel, J. Am. Chem. Soc. 130 (2008) 13301–13309, https://doi.org/10.1021/ja803188c.
[7] J. Chevalier, M. Malléa, J.-M. Pagès, Comparative aspects of the diffusion of norfloxacin, cefepime and spermine through the F porin channel of Enterobacter cloacae, Biochem. J. 348 (2000) 223, https://doi.org/10.1042/0264-6021:3480223.
[8] J. Cama, H. Bajaj, S. Pagliara, T. Maier, Y. Braun, M. Winterhalter, U.F. Keyser, Quantification of fluoroquinolone uptake through the outer Membrane channel OmpF of *Escherichia coli*, J. Am. Chem. Soc. 137 (2015) 13836–13843, https://doi.org/10.1021/jacs.5b08960.
[9] O. Cramariuc, T. Rog, M. Javanainen, L. Monticelli, A.V. Polishchuk, I. Vattulainen, Mechanism for translocation of fluoroquinolones across lipid membranes, Biochim. Biophys. Acta BBA - Biomembr. 1818 (2012) 2563–2571, https://doi.org/10.1016/j.bbamem.2012.05.027.
[10] P. Neves, E. Berkane, P. Gameiro, M. Winterhalter, B. de Castro, Interaction between quinolones antibiotics and bacterial outer membrane porin OmpF, Biophys. Chem. 113 (2005) 123–128, https://doi.org/10.1016/j.bpc.2004.08.004.
[11] J. Cama, M. Schaich, K. Al Nahas, S. Hernández-Ainsa, S. Pagliara, U.F. Keyser, Direct optofluidic measurement of the lipid permeability of fluoroquinolones, Sci. Rep. 6 (2016), https://doi.org/10.1038/srep32824.
[12] A. Grancelli, A. Morros, M.E. Cabañas, Ò. Domènech, S. Merino, J.L. Vázquez, M. T. Montero, M. Viñas, J. Hernández-Borrell, Interaction of 6-fluoroquinolones with dipalmitoylphosphatidylcholine monolayers and liposomes, Langmuir. 18 (2002) 9177–9182, https://doi.org/10.1021/la025837h.
[13] S. Correia, P. Poeta, M. Hébraud, J.L. Capelo, G. Igrejas, Mechanisms of quinolone action and resistance: where do we stand? J. Med. Microbiol. 66 (2017) 551–559, https://doi.org/10.1099/jmm.0.000475.
[14] A. Albini, S. Monti, Photophysics and photochemistry of fluoroquinolones, Chem. Soc. Rev. 32 (2003) 238, https://doi.org/10.1039/b209220b.
[15] S.V. Blokhina, A.V. Sharapova, M.V. Ol'khovich, T.V. Volkova, G.L. Perlovich, Solubility, lipophilicity and membrane permeability of some fluoroquinolone antimicrobials, Eur. J. Pharm. Sci. 93 (2016) 29–37, https://doi.org/10.1016/j.ejps.2016.07.016.
[16] G.-M. Cárdenas-Youngs, J.-L. Beltrán, Dissociation constants and octanol–water partition equilibria for several fluoroquinolones, J. Chem. Eng. Data 60 (2015) 3327–3332, https://doi.org/10.1021/acs.jced.5b00556.
[17] G.S.V. Muniz, L.R. Teixeira, S.R.W. Louro, Interaction of the antibiotic norfloxacin with ionic micelles: pH-dependent binding, Eur. Biophys. J. 43 (2014) 477–483, https://doi.org/10.1007/s00249-014-0978-5.
[18] H. Bensikaddour, K. Snoussi, L. Lins, F. Van Bambeke, P.M. Tulkens, R. Brasseur, E. Goormaghtigh, M.-P. Mingeot-Leclercq, Interactions of ciprofloxacin with DPPC and DPPG: fluorescence anisotropy, ATR-FTIR and 31P NMR spectroscopies and conformational analysis, Biochim. Biophys. Acta BBA - Biomembr. 1778 (2008) 2535–2543, https://doi.org/10.1016/j.bbamem.2008.08.015.
[19] M. Ferreira, P. Gameiro, Ciprofloxacin metalloantibiotic: an effective antibiotic with an influx route strongly dependent on lipid interaction? J. Membr. Biol. 248 (2015) 125–136, https://doi.org/10.1007/s00232-014-9749-6.
[20] M. Fresta, S. Guccione, A.R. Beccari, P.M. Furneri, G. Puglisi, Combining molecular modeling with experimental methodologies: mechanism of membrane permeation and accumulation of ofloxacin, Bioorg. Med. Chem. 10 (2002) 3871–3889, https://doi.org/10.1016/S0968-0896(02)00350-4.
[21] S. Ortiz-Collazos, P.H.S. Picciani, O.N. Oliveira, A.S. Pimentel, K.J. Edler, Influence of levofloxacin and clarithromycin on the structure of DPPC monolayers, Biochim. Biophys. Acta BBA - Biomembr. 1861 (2019) 182994, https://doi.org/10.1016/j.bbamem.2019.05.016.
[22] S. Ortiz-Collazos, E.D. Estrada-López, A.A. Pedreira, P.H.S. Picciani, O.N. Oliveira, A.S. Pimentel, Interaction of levofloxacin with lung surfactant at the air-water interface, Colloids Surf. B Biointerfaces. 158 (2017) 689–696, https://doi.org/10.1016/j.colsurfb.2017.07.066.
[23] A. Khondker, R.-C. Bider, I. Passos-Gastaldo, G.D. Wright, M.C. Rheinstädter, Membrane interactions of non-membrane targeting antibiotics: the case of aminoglycosides, macrolides, and fluoroquinolones, Biochim. Biophys. Acta BBA - Biomembr. 2021 (1863) 183448, https://doi.org/10.1016/j.bbamem.2020.183448.
[24] D. Marsh, Handbook of Lipid Bilayers, 2nd ed, CRC Press, Taylor & Francis Group, Boca Raton, FL, 2013.
[29] J. Coelho (Ed.), Drug Delivery Systems: Advanced Technologies Potentially Applicable in Personalised Treatment, Springer Netherlands, Dordrecht, 2013, https://doi.org/10.1007/978-94-007-6010-3.
[30] X. Zhang, P. Sun, R. Bi, J. Wang, N. Zhang, G. Huang, Targeted delivery of levofloxacin-liposomes for the treatment of pulmonary inflammation, J. Drug Target. 17 (2009) 399–407, https://doi.org/10.1080/10611860902795407.
[31] E. Kłosińska-Szmurło, M. Grudzień, F.P.K. Betlejewska-Kielak Monika, J. Biernacka, A.P. Mazurek, Acta chimica slovenica, physicochem. prop. lomefloxacin levofloxacin moxifloxacin relev, Biopharm. Classif. Syst. 61 (2014) 827–834.
[32] G. Rouser, A.N. Siakotos, S. Fleischer, Quantitative analysis of phospholipids by thin-layer chromatography and phosphorus analysis of spots, Lipids. 1 (1966) 85–86, https://doi.org/10.1007/BF02668129.
[33] T.A. Enoki, I. Moreira-Silva, E.N. Lorenzon, E.M. Cilli, K.R. Perez, K.A. Riske, M. T. Lamy, Antimicrobial peptide K^0-W^6-Hya1 induces stable structurally modified lipid domains in anionic membranes, Langmuir. 34 (2018) 2014–2025, https://doi.org/10.1021/acs.langmuir.7b03408.
[34] G.S. Vignoli Muniz, L.I. De la Torre, E.L. Duarte, E.N. Lorenzón, E.M. Cilli, A. Balan, M.T. Lamy, Interaction of synthetic antimicrobial peptides of the Hylin a1 family with models of eukaryotic structures: Zwitterionic membranes and DNA, Biochem. Biophys. Rep. 24 (2020) 100827, https://doi.org/10.1016/j.bbrep.2020.100827.
[35] H.M. McConnell, W.L. Hubbell, Molecular motion in spin-labeled phospholipids and membranes, J. Am. Chem. Soc. 93 (1971) 314–326, https://doi.org/10.1021/ja00731a005.
[36] D. Marsh, in: E. Grell (Ed.), Membrane Spectroscopy, Electron spin resonance: Spin Labels, Chapter 2, Springer Berlin Heidelberg, Berlin, Heidelberg, 1981, https://doi.org/10.1007/978-3-642-81537-9.
[37] J.H.K. Rozenfeld, E.L. Duarte, T.R. Oliveira, M.T. Lamy, Structural insights on biologically relevant cationic membranes by ESR spectroscopy, Biophys. Rev. 9 (2017) 633–647, https://doi.org/10.1007/s12551-017-0304-4.
[38] J.R. Lakowicz (Ed.), Principles of Fluorescence Spectroscopy, Springer US, Boston, MA, 2006, https://doi.org/10.1007/978-0-387-46312-4.
[39] A. Mendonça, A.C. Rocha, A.C. Duarte, E.B.H. Santos, The inner filter effects and their correction in fluorescence spectra of salt marsh humic matter, Anal. Chim. Acta 788 (2013) 99–107, https://doi.org/10.1016/j.aca.2013.05.051.
[40] B. Valeur, Molecular Fluorescence: Principles and Applications, Wiley-VCH, Weinheim, New York, 2002.
[41] T. Heimburg, Thermal Biophysics of Membranes, Weinheim, Wiley-VCH Verlag, 2007.
[42] U. Hubicka, P. Żmudzki, P. Talik, B. Żuromska-Witek, J. Krzek, Photodegradation assessment of ciprofloxacin, moxifloxacin, norfloxacin and ofloxacin in the presence of excipients from tablets by UPLC-MS/MS and DSC, Chem. Cent. J. 7 (2013), https://doi.org/10.1186/1752-153X-7-133.
[43] J. Nisar, M. Iqbal, M. Iqbal, A. Shah, M.S. Akhter, R.A. Khan Sirajuddin, I. Uddin, L. A. Shah, M.S. Khan, Decomposition kinetics of levofloxacin: drug-excipient interaction, Z. Für Phys. Chem. 234 (2020) 117–128, https://doi.org/10.1515/zpch-2018-1273.
[44] K.A. Riske, R.P. Barroso, C.C. Vequi-Suplicy, R. Germano, V.B. Henriques, M. T. Lamy, Lipid bilayer pre-transition as the beginning of the melting process, Biochim. Biophys. Acta BBA - Biomembr. 1788 (2009) 954–963, https://doi.org/10.1016/j.bbamem.2009.01.007.
[45] F.C.L. Luiz, S.R.W. Louro, Acid–base equilibrium of drugs in time-resolved fluorescence measurements: theoretical aspects and expressions for apparent pKa shifts, J. Photochem. Photobiol. Chem. 222 (2011) 10–15, https://doi.org/10.1016/j.jphotochem.2011.03.006.
[46] A. Kaur, I.A. Khan, P.K. Banipal, T.S. Banipal, Deciphering the complexation process of a fluoroquinolone antibiotic, levofloxacin, with bovine serum albumin in the presence of additives, Spectrochim. Acta A Mol. Biomol. Spectrosc. 191 (2018) 259–270, https://doi.org/10.1016/j.saa.2017.10.017.
[47] N.C. Santos, M. Prieto, M.A.R.B. Castanho, Quantifying molecular partition into model systems of biomembranes: an emphasis on optical spectroscopic methods,

Biochim. Biophys. Acta BBA - Biomembr. 1612 (2003) 123–135, https://doi.org/10.1016/S0005-2736(03)00112-3.
[48] A. Konstantinidi, M. Chountoulesi, N. Naziris, B. Sartori, H. Amenitsch, G. Mali, T. Cendak, M. Plakantonaki, I. Triantafyllakou, T. Tselios, C. Demetzos, D. Busath, T. Mavromoustakos, A. Kolocouris, Influenza A M2 Spans the Membrane Bilayer, Perturbs its Organization and Differentiates the Effect of Amantadine and Spiro [pyrrolidine-2,2′-adamantane] AK13 on Lipids, 2019, https://doi.org/10.26434/chemrxiv.8969678.v1.
[49] P. Devaux, H. McConnell, Lateral diffusion in spin-labeled phosphatidylcholine multilayers, J. Am. Chem. Soc. 94 (1972) 4475–4481, https://doi.org/10.1021/ja00768a600.
[50] P. Devaux, C.J. Scandella, H.M. McConnell, Spin-spin interactions between spin-labeled phospholipids incorporated into membranes, J. Magn. Reson. 1969 (9) (1973) 474–485, https://doi.org/10.1016/0022-2364(73)90190-X.
[51] J.H.K. Rozenfeld, E.L. Duarte, L.R.S. Barbosa, M.T. Lamy, The effect of an oligonucleotide on the structure of cationic DODAB vesicles, Phys. Chem. Chem. Phys. 17 (2015) 7498–7506, https://doi.org/10.1039/C4CP05652C.
[52] D.F. Evans, H. Wennerström, The Colloidal Domain: Where Physics, Chemistry, Biology, and Technology Meet, 2nd ed, Wiley-VCH, New York, 1999.
[53] K.A. Riske, O.R. Nascimento, M. Peric, B.L. Bales, M.T. Lamy-Freund, Probing DMPG vesicle surface with a cationic aqueous soluble spin label, Biochim. Biophys. Acta BBA - Biomembr. 1418 (1999) 133–146, https://doi.org/10.1016/S0005-2736(99)00019-X.
[54] B.K. Paul, N. Ghosh, S. Mukherjee, Interplay of multiple interaction forces: binding of norfloxacin to human serum albumin, J. Phys. Chem. B 119 (2015) 13093–13102, https://doi.org/10.1021/acs.jpcb.5b08147.
[55] S. Sortino, Selective entrapment of the cationic form of norfloxacin within anionic sodium dodecyl sulfate micelles at physiological pH and its effect on the drug photodecomposition†, Photochem. Photobiol. 82 (2006) 64, https://doi.org/10.1562/2005-06-01-RA-560.
[56] S. Sortino, G. De Guidi, S. Giuffrida, Drastic photochemical stabilization of lomefloxacin through selective and efficient self-incorporation of its cationic form in anionic sodium dodecyl sulfate (SDS) micelles, New J. Chem. 25 (2001) 197–199, https://doi.org/10.1039/b008257k.